MARMARA UNIVERSITY
FACULTY OF ENGINEERING

IMPROVEMENT OF SOLAR ENERGY SYSTEMS FOR FIXED WING AIRCRAFT & SPACE SYSTEMS

Mehmet Can ADSIZ, Hacı Enes BESYAPRAK

GRADUATION PROJECT REPORT

Department of Mechanical Engineering

Supervisor

Doç. Dr. Barış Yılmaz

ISTANBUL, 2023

MARMARA UNIVERSITY
FACULTY OF ENGINEERING

Improvement of Solar Energy Systems for Fixed Wing Aircraft & Space Systems by

Mehmet Can ADSIZ, Hacı Enes BEŞYAPRAK
June, 2023, Istanbul

SUBMITTED TO THE DEPARTMENT OF MECHANICAL ENGINEERING IN PARTIAL FULFILLMENT OF THE REQUIREMENTS FOR THE DEGREE

OF

BACHELOR OF SCIENCE

AT

MARMARA UNIVERSITY

Signature of Author(s) .....
Department of Mechanical Engineering

Certified By .....
Project Supervisor, Department of Mechanical Engineering

Accepted By ....
Head of the Department of Mechanical Engineering

ACKNOWLEDGEMENT

First of all, we would like to thank our supervisor Doç. Dr. Barış YILMAZ, for the valuable guidance and advice on preparing this thesis and giving me moral and material support.

June, 2023 **Mehmet Can ADSIZ, Hacı Enes Beşyaprak**

CONTENT

ABSTRACT

Solar energy is increasingly gaining importance as a sustainable and clean energy source in today's world. It holds exciting potential, particularly in applications such as unmanned aerial vehicles and space systems. Utilizing solar energy-based designs in these systems is crucial for enhancing energy efficiency and providing a sustainable energy source with long mission durations. Moreover, the use of solar energy-based systems has the potential to reduce energy costs and optimize energy consumption. In this study, a design was developed using GaAs solar cells with the primary goal of improving energy efficiency and providing a continuous energy source for aircraft.

To achieve this objective, a literature review was conducted to examine previous studies in the field. An appropriate airfoil was selected based on aerodynamic analyses that aligned with the required altitude and flight speeds. Subsequently, efforts were made to optimize the placement of solar cells on the wings of the unmanned aerial vehicle system. Power requirements and power consumption calculations were performed to analyze the energy efficiency of the system. Based on the conducted studies, critical aspects of the design were addressed to meet the energy demands.

Overall, this study highlights the increasing significance of solar energy as a sustainable and clean energy source in various applications, particularly in the field of unmanned aerial vehicles and space systems. By harnessing solar energy, the aim is to enhance energy efficiency and provide a continuous energy source for aircraft.

Keywords — Solar Energy, GaAs solar cell, Energy optimization, Airfoil selection, Solar cell placement, Unmanned Aerial Vehicle (UAV)

SYMBOLS

θ :**Angle of incidence**

G_{sc}: **Solar constant**

δ: **Declination angle**

n: **Day number**

ϕ: **Latitude angle**

R_b: **Geometric factor**

I_0: **Hourly integrated solar irradiation**

I_{est}: **Estimated solar irradiation**

η_{cell}: **Solar cell efficiency**

N: **Number of daylight hours**

ω :**Hour angle**

η: **Efficiency**

P **:Power**

V **: Voltage**

I **: Current**

E **: Energy**

P : **Density**

W **:Watt (Unit of Power)**

m**: Meter (Unit of length)**

Kg **: Kilogram (Unit of mass)**

s **:Second (Unit of time)**

$^{\circ}C$**: Degree Celsius (Unit of temperature)**

ABBREVIATIONS

UAV **:** Unmanned Air Vehicle

C_L **:** Lift Coefficient

C_D **:** Drag Coefficient

C_L/ C_D **:** Lift to Drag Ratio

Alpha **:** Angle of Attack

GaAs **:** Gallium Arsenide

CAD **:** Computer-Aided Design

PV **:** Photovoltaic

DC **:**Direct Current

AC **:**Alternating Current

HVAC **:**Heating, Ventilation, and Air Conditioning

Li-Ion **:**Lithium-Ion

FIGURE LIST

LIST OF TABLES

1 INTRODUCTION

The increasing concern over climate change has led to a renewed focus on the development and implementation of clean energy sources. Among the various forms of clean energy, “Solar Energy” has emerged as a valuable area of research and investment. The utilization of solar cells for energy production has significant advancement in recent years, with improvements in technology leading to increased energy efficiency, reduced production cost.

Solar powered aircraft systems have been studied for 40 years. The improvement of solar cell technology by their efficiency level is given in figure 1.1 below [1]. Furthermore, GaAs and Amorf-Si based solar cells with around 30% efficiency are recently. Although the cost of this technology might be quite high for today, yet costs are continuously decreasing and will be much affordable in the near future.

This research project aims to design a solar cell system that can be integrated into fixed-wing aircraft and space systems for use in both the defense industry and civilian aviation. The current widespread use of the internal combustion engines in aircrafts limits the flight time of vehicles and can cause issues during long flights at high altitudes. Thereby, the designed solar cell system has the potential to overcome these limitations by providing a sustainable power input to the system without the need for fuel resupply. Additionally, the energy needs of various equipment on the aircraft can also be met by these cells.

In line with all these objectives, the needed design study is begun by determining the maximum number and area of solar cells that can be placed on the wing surface area. All the necessary calculations are made to determine the energy that can be produced by the solar cells. Furthermore, the number and placement of Li-ion batteries are depicted in this study. The aim here is to determine a battery positioning that minimizes the differences between optimum and working temperatures which can affect the life and performance of the batteries and provides a regular temperature distribution.

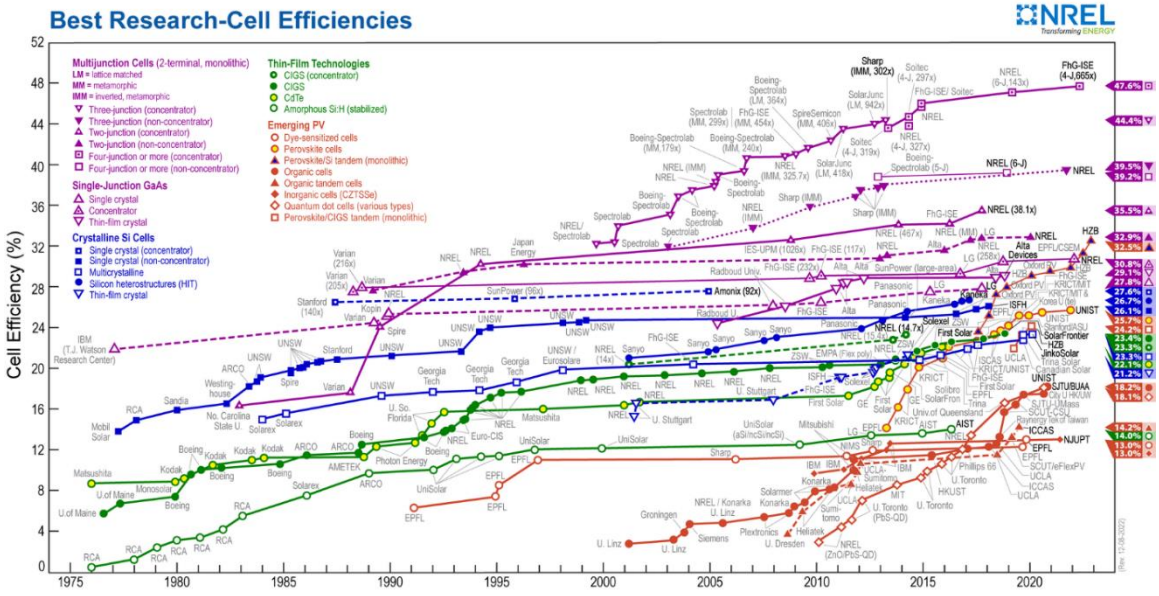

Figure 1.1 Efficiency of Solar Cells over years [1]

1.1 Historical Review of Solar Powered UAV (literature survey)

It is important to note that there have been prior studies conducted on solar powered UAV systems. However, history of solar powered flight began in 1974 with Sunrise-1 [2]. It had a 32 ft wingspan, 90 ft^2 wing area and it was 27.6 Ib airplane. Solar cells produced 450-watt power, which allowed Sunrise 1 to fly 20 minutes. Later, in 1975 some improvements were performed on the airplane such as decreasing its weight and increasing its solar cell quantity. Solar cells had 14% efficiency and delivered 600 watts of energy.

(at an altitude of around 100 m during its inaugural flight. It had a wingspan of 9.76 m, weighed 12.25 kg and the power output of the 4096 solar cells was 450 W [ref: R. J. Boucher, History Of Solar Flight, AIAA Paper 84-1429, June 1984].)

Figure 1.2 Sunrise-1

The study of manned solar powered flight was initiated following the successful implementation of solar power on model airplanes. In 1978, the first solar powered airplane, Solar One, was designed by Britons David Williams. This aircraft had a 68 ft wingspan and a 258 ft^2 wing area, with a total weight of 229 lb and a service ceiling of approximately 79 ft. The designers utilized nickel-cadmium batteries to power the aircraft.

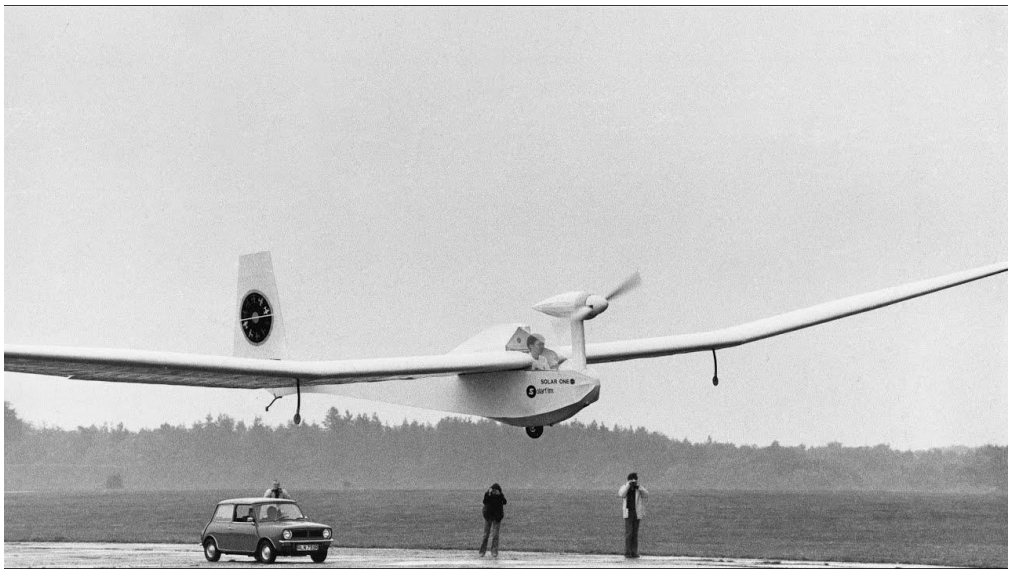

Figure 1.3 Solar One [3]

On the other side of the Atlantic, Helmut Bruss was working in Germany on a solar model airplane in summer 1975 without having heard anything about Boucher's project. Unluckily, due to overheating of the solar cells on his model, he didn't achieve level flight and finally the first one in Europe was his friend 'Fred Militky', one year later, with "Solaris". On the 16th of August 1976, it completed three flights of 150 seconds reaching the altitude of 50 m[4].

Figure 1.4 Solaris,1976

Another crucial solar powered aircraft study is designed by Aerovironment and Paul MacCready. Gossamer Condor and Gossamer Albatros, which were human powered airplanes, were designed in 1977 and 1979 respectively by Paul MacCready. Success of Solar One gave an idea for converting Gossamer airplane series to a solar powered airplane called Gossamer Penguin, Figure 1.5.

The Penguin was a three-quarters scale version of the Gossamer Albatross II, and had a 71 ft.(21.64 meter) wingspan and a weight, without pilot, of 68 lb (31 kg). The powerplant was an AstroFlight Astro-40 electric motor, driven by a 541-watt solar panel consisting of 3920 solar cells. Initial test flights were performed using a 28 cell NiCad battery pack instead of a panel. The test pilot for these flights was MacCready's 13 year old son Marshall, who weighed 80 lb (36 kg) [5].

Figure 1.5 Gossamer Penguin [5]

However, the Gossamer Penguin was not safe for a pilot flying at more that a few feet. The Dupont Company, encouraged by the results of the Gossamer Penguin, sponsored MacCready for building a new solar airplane that would cross the English Channel. The Solar Challenger was a 14.2 m wingspan highwing monoplane with 16128 solar cells offering 2500 Watt at sea level. On July 7, 1981, it flew from Puntoise-Cormeilles near Paris to Manston RAF Base near London in 5 hours 23 minutes covering 262.3 km, with solar energy as its sole power source and no onboard energy storage system [5].

Figure 1.6 Solar Challenger, 1981[5]

In 1986, Eric Raymond started the design of the Sunseeker in the United States**.** The Solar Riser in 1979, Solar Challenger two years later and a meeting with Günter Rochelt in Germany had convinced him to build his own manned solar-powered aircraft. At the end of 1989, the Sunseeker was test flown as a glider and during August 1990, it crossed the USA in 21 solar powered flights with 121 hours in the air [5].

Figure 1.7Sunseeker [5]

Icare 2, which was designed in 1996 by Prof Rudolf Voit-Nitschmann from Stuttgart University was the fastest solar powered airplane in 1996. It had a 109.3 ft/s maximum speed [6].

Figure 1.8 Icare 2

In the late 1990s, design considerations for solar powered aircraft underwent changes as scientists explored the use of fuel cell technology for perpetual endurance. Despite the potential benefits, this technology was not yet advanced enough to be implemented. By 2001, the focus shifted towards reaching higher altitudes, resulting in the design of the Helios aircraft by NASA. This aircraft set a record by reaching an altitude of 96000 ft and flying for approximately 40 minutes at that height. Despite the advantage of low wind speeds at high altitudes, the low air density presented challenges in terms of cooling the solar cells. The Helios aircraft was designed with the goal of attaining perpetual endurance, however, it suffered a serious crash in 2003 due to structural vibration causing wing failure [7].

Figure 1.9 NASA Helios

Solar Impulse, a Swiss project, is another important solar power airplane application. It performed its first flight in 2009. Solar Impulse 1 had 208 ft wingspan and weighed only 3528 lb, Figure 1.10. It had 4 electric motors and efficient lithium-ion batteries which weighed approximately 1446 lb and delivered 21 kWh power each. The first design could perform 36 hours of flight. Then, the firm decided to improve the first design and in 2014 Solar Impulse design was begun. It had a 236 ft wingspan and weighed about 5070 lb. The cruise speed of first design was 64 ft/s; on the other hand, the cruise speed of Solar Impulse 2 was 70.1 ft/s. It has not become an operational airplane yet since some problems aroused in the batteries [7].

Figure 1.10 Solar Impulse 2 [7]

The last important application is the Boeing Solar Eagle. It is an ongoing project. The aim of the project is to attain one month endurance. It uses fuel cell to provide power at night. It has 400 ft wingspan and has the capacity to carry 1103 lb payload. [8]

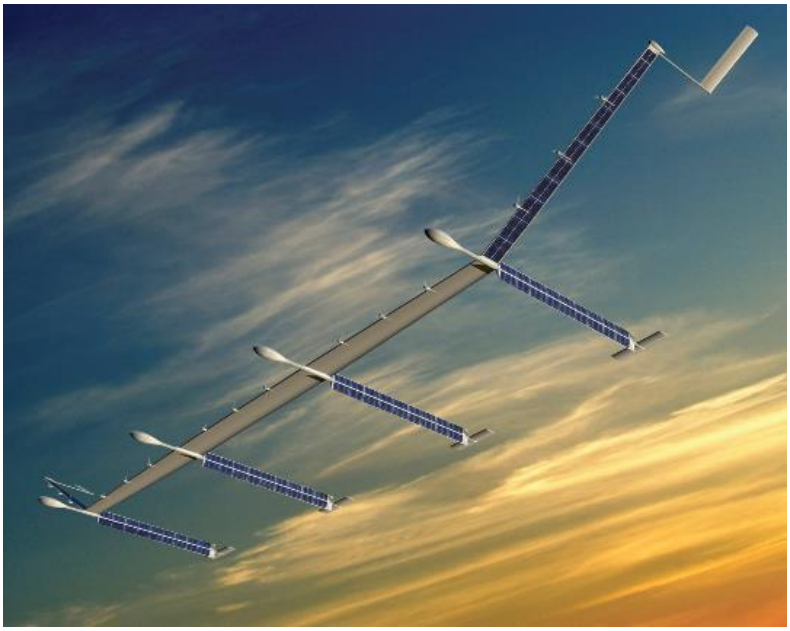

Figure 1.11 Boeing Solar Eagle [7]

All these systems have also been used for military purposes. Their contributions to the defense industry are as following examples:

In 1998, the HALE UAV Global Hawk, a surveillance unmanned aircraft, was designed, and began flying successfully. The Global Hawk had a 131 ft wingspan and weighed 32250 lb. It was capable of flying approximately 32 hours at an altitude of 65000 ft.

The Heron TP, also known as the AIA Eitan, was developed in 2004. This twin boom pusher aircraft had a wingspan of 85.3 ft, a payload capacity of 4410 lb, and a 9000-kW power plant. During test flights, the Heron TP achieved a 70-hour endurance and a service ceiling of 15 km. The Heron TP continues to be in service [7].

Figure 1.12 Global Hawk and Heron TP (in order)

Designing aircraft to fly at altitudes between 45000 ft and 65000 ft presents significant challenges, as the low air density and temperature at these heights pose restrictions. Subsystems require heating systems to withstand harsh weather conditions. At an altitude of 65000 ft, air density decreases by a factor of 14 and pressure decreases by 18 times in comparison to sea level conditions, with temperatures dropping as low as -80°C.

Altitude (ft)	**Temperature (ºC)**	**Pressure (lb/ft^2)**	**Density (10^{-3} slugs/ft^3)**	**Dynamic Viscosity (10^{-7} lb.s/ft^2)**	**Speed of sound (ft/s)**
0	15.0	2116.2	2.38	3.74	1115.5
15000	-21.9	1194.8	1.50	3.43	1049.9
30000	-44.4	629.7	0.089	3.11	980.95
45000	-56.5	309.5	0.0462	2.97	968
65000	-56.5	118.9	0.0178	2.97	968
80000	-52.2	58.5	0.0086	3.02	968

Table 1 Air Conditions Variations with Altitude [7]

1.2 Solar Cells

Photovoltaic or solar cells are electronic components that use light from the sun to generate electricity. They are essential in the realm of renewable energy since they give homes, businesses, and communities a reliable and safe supply of electricity. A core component of solar panels, which are formed of numerous individual cells linked together to improve their power production, are solar cells.

Figure 1.13 Solar Panel

The heart of a solar cell is the photovoltaic effect. The photovoltaic effect, the theoretical underpinning of solar cell technology, was discovered in the 19th century. The first solar cell was constructed by Charles Fritts in 1877 by using junctions formed by coating the semiconductor selenium with an ultra-thin layer of gold. Fritts's devices were very inefficient, transforming less than 1 percent of the absorbed light into electrical energy[10]. However, Bell Labs did not produce the first useful solar cell until the 1950s. Since then, technological developments have significantly increased the effectiveness and accessibility of solar cells. Solar cells are now widely used for domestic, industrial, and commercial purposes. They are also an essential part of satellite and space mission power systems.

Figure 1.14 showing a simple silicon solar cell. When sunlight hit the surface of solar cell it creates charge carriers as electron these electrons are at higher state of energy, allowing them to flow freely and create an electrical current. Solar cells are constructed from two layers of semiconductor material, with one layer having an excess of electrons and the other layer having a deficit of electrons. When sunlight is absorbed by the cell, it releases electrons, which flow through an external circuit and generate an electrical current. The electrical current produced by a single solar cell is relatively small, but by connecting multiple cells together, the power output can be increased.

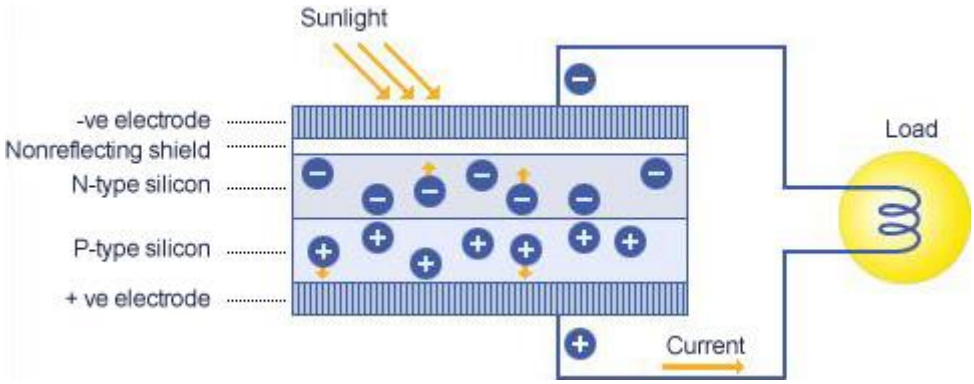

Figure 1.14 Representation of working principle of solar cells

Silicon is the very important material in photovoltaic technology due to it is abundance and high efficiency. The basic structure of silicon solar cells occurs a thin layer of n-type (negative) silicon and a thin layer of p-type (positive) silicon. The p-n junction, which is generated by these two layers, is where the electrical current is generated. There are mainly two type of silicon solar cell these are Monocrystalline and Polycrystalline.

Monocrystalline Silicon Cells are made from a single, high-purity crystal of silicon and are considered to be the most efficient type of silicon solar cell. Monocrystalline solar cells are made from a single, continuous crystal of silicon. They are manufactured by slicing a cylindrical ingot of pure silicon into thin wafers. The ingot is grown in a high-temperature furnace, where a single silicon crystal is formed and then slowly pulled from a pool of molten silicon. The resulting ingot has a cylindrical shape, and it is then cut into thin wafers using a wire saw.

Polycrystalline solar cells, also known as multi crystalline cells, are made from many small crystals of silicon. They are manufactured by melting raw silicon and pouring it into a mold to form a block of silicon. This block is then sliced into thin wafers using a wire saw.

The manufacturing process of polycrystalline solar cell is more and simple and less expensive than monocrystalline solar cells, which it results lower cost. However, it is slightly less efficient than monocrystalline.

There is another category for solar cell. It is Thin-Film Solar Cells These are made from a thin layer of semiconductor material on a substrate, such as glass or metal, and are the least efficient type of solar cell but also the most flexible and inexpensive. However, semiconductor material could change it is cost and efficiency rate we will work on Gallium Arsenide Solar Cells.

Gallium Arsenide Solar Cells use Gallium arsenide as a semiconductor material. Gallium arsenide solar cells work on a similar principle to silicon solar cells, but the p-n junction is formed by combining two different semiconductor materials, gallium arsenide and gallium phosphide.

Light photons are absorbed by the gallium arsenide layer, which produces electron-hole pairs. The p-n junction's electric field subsequently separates the electron-hole pairs. The gallium phosphide layer serves as a window layer to boost the efficiency of the cell by allowing lighter to enter.

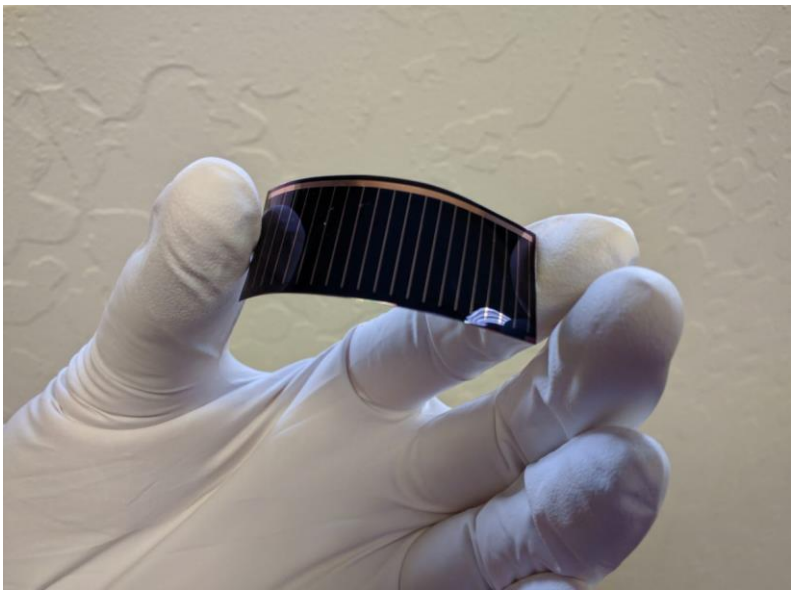

Figure 1.15 GaAs Solar Cell [11]

Compared to silicon solar cells, gallium arsenide solar cells are more efficient because they can absorb a wider variety of electromagnetic spectrum and produce more electron-hole pairs. They are generally utilized in areas where great efficiency is required, such as concentrated solar systems and space applications, but since they are more expensive to create.

Gallium arsenide (GaAs) solar cells are an alternative to traditional silicon solar cells and offer higher efficiency in converting sunlight into electricity. GaAs solar cells have the ability to absorb a wider range of the electromagnetic spectrum, allowing them to generate more electron-hole pairs compared to silicon cells. This increased efficiency makes GaAs solar cells ideal for applications that require high performance, such as concentrated solar systems and space missions. However, the production cost of GaAs solar cells is generally higher than that of silicon cells.[12].

In the construction of GaAs solar cells, the p-n junction is formed by combining two different semiconductor materials, gallium arsenide and gallium phosphide. When light photons strike the gallium arsenide layer, they create electron-hole pairs. The electric field at the p-n junction then separates these pairs. To further enhance the cell's efficiency, a gallium phosphide layer is incorporated as a window layer, allowing lighter photons to enter and contribute to the electricity generation process.

Compared to silicon solar cells, the advantages of gallium arsenide solar cells lie in their ability to absorb a broader range of the electromagnetic spectrum and generate more electron-hole pairs. These features make them highly suitable for applications where exceptional efficiency is required. However, their higher production cost often limits their use to specialized and cost-tolerant applications such as concentrated solar systems and space missions. [13]

1.3 Working Principle of Li-ion Battery

Batteries are an essential component of modern technology, powering everything from cell phones and laptops to electric cars and renewable energy systems. Batteries store electrical energy that can be used as needed, providing a convenient and portable source of power. There are many different types of batteries available, each with its own set of strengths and limitations. Battery is formed of one or more electrochemical cells that produce an electron flow through a chemical process. The battery cell is consisting of positive and negative electrode plates which are insulated from each other, and an electrolyte that provides conductivity between the plates. Both groups of electrodes are connected to two terminals. These cells can store energy at very low electrical potentials.[14].

Figure 1.16 Rechargeable Li-İon Batteries

The working principle of a Li-ion battery is based on the movement of lithium ions between the positive and negative electrodes as the battery is charged and discharged. When the battery is charged, lithium ions are attracted to the negative electrode, and when the battery is discharged, the ions are attracted to the positive electrode. This creates an electrical current that provides power to the device. The performance of a Li-ion battery is determined by a number of factors, including the materials used for the electrodes, the electrolyte used to transport the ions, and the design of the battery itself.

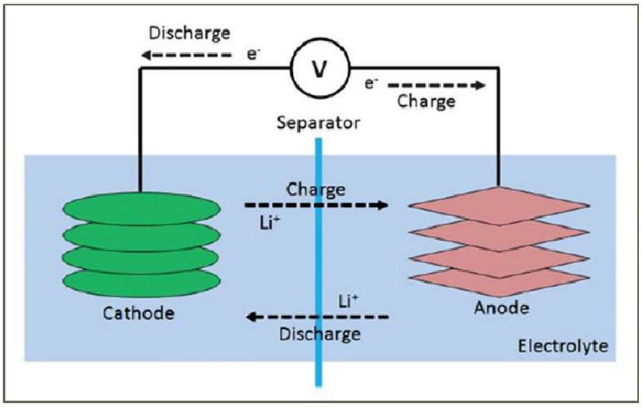

Figure 1.17 Show how Li-ion battery charge and discharge[15].

2 METHODOLOGY

2.1 Preliminary Design

Most of the airplane designs are evolutionary not revolutionary, hence choosing suitable competitor aircraft and specifying applicable requirements is very important. The conceptual design begins with requirements.

The main objective of the UAV in this design is to perform border surveillance, providing real-time video and image data of the monitored area. To achieve this goal, it is crucial to determine the appropriate energy and geometrical parameters for the UAV. The supporting company provided vital information and technical specifications that were taken into account when designing the UAV's power and geometry systems.

2.1.1 Requirement Table

Based on the in-depth literature review conducted during the creation of the requirement matrix, two matrices were developed: one based on the literature data, and another provided by the supporting company, which helped to identify our requirements.

Mass	**Wing area**	**Wingspan**	**Aspect Ratio**	**Max. needed power**	**Endurance**	**Payload**	**Rate of climb**	**Service altitude**
[kg]	**[m^2]**	**[m]**	-	**[kW]**	**[hour]**	**[kg]**	**[m/sec]**	**[ft]**
9.65	3.77	7	13	-	-	5	-	10 000

Table 2 Requirement Matrix from literature [16]

Mass	**Wing area**	**Wingspan**	**Aspect Ratio**	**Max. needed power**	**Endurance**	**Payload**	**Rate of climb**	**Service altitude**
[kg]	**[m^2]**	**[m]**	-	**[kW]**	**[hour]**	**[kg]**	**[m/sec]**	**[ft]**
200 kg	TBC	4-8 (predicted)	12-13	TBC	Solar day long	5	1	3 000

Table 2 Requirement Matrix from supporting company.

As additional; Stall and cruise speeds are given as 20 m/sec and 31 m/sec. Also aspect ratio of design shall be 12-13

2.2 Mission Profile

The mission profile of the unmanned aerial vehicle (UAV) in this design is intended to primarily serve as an observation platform along the border. Through analysis of information provided by the supporting company, calculations will be performed to determine the necessary energy and geometry requirements for the UAV.

The energy calculations were performed by considering the UAV's weight, size, and mission requirements. These calculations included estimating the amount of energy needed to power the propulsion system, sensors, communication equipment, and other electronic components. The geometrical calculations involved determining the optimal wingspan, aspect ratio, and airfoil shape for the UAV, which would allow for efficient flight performance while meeting the mission's requirements.

By utilizing the information provided by the supporting company and conducting in-depth literature reviews, a comprehensive requirement matrix was developed. This matrix defined the necessary specifications and parameters for the UAV's power and geometrical systems. The requirement matrix served as a critical guide during the UAV's design and development stages and ensured that the UAV met the necessary specifications for successful border surveillance operations.

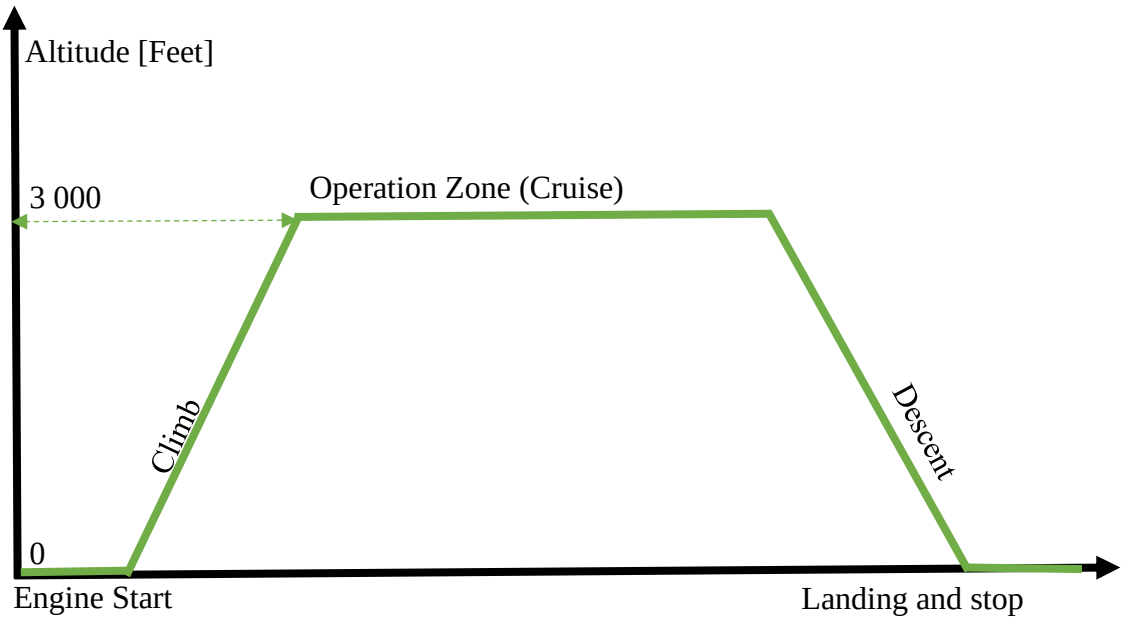

Figure 2.1Mission Profile from TAI

2.3 Airfoil and Wing Platform Selection

In addition to energy and geometrical considerations, the selection of an appropriate wing design is a crucial factor in the successful operation of a solar-powered aircraft. A well-designed wing not only needs to have good aerodynamic characteristics, but it must also be suitable for the insertion of solar cells onto its top surface. In the case of this solar-powered UAV, a high cantilever wing design has been chosen. This design was primarily chosen for its simplicity and ability to provide enough clearance for a skid landing. Additionally, a high wing design offers better lateral stability, which is critical since there will be minimal stabilizing devices on this type of UAV.

When designing the wing, the team considered several key factors. One of these factors was the aspect ratio of the wing. A high aspect ratio wing was chosen to maximize the lift-to-drag ratio, which is essential for achieving the required range and endurance. The wing's surface area was also optimized to ensure that it provided enough space for solar cells while still maintaining adequate structural strength.

In summary, the selection of an appropriate wing design is critical for the successful operation of a solar-powered UAV. Through careful consideration of factors such as wing geometry, surface area, and airfoil shape, the team was able to select a high cantilever wing design that meets the UAV's requirements for simplicity, clearance, lateral stability, and energy efficiency.

2.3.1 Sweep Angle

Sweep angle is the angle between the leading edge of an aircraft wing and its longitudinal axis. It affects the wing's aerodynamic performance, including drag reduction at high speeds, lift-to-drag ratio, and stability characteristics. Swept-back wings tend to be more stable at high speeds but have lower lift-to-drag ratios, while swept-forward wings can provide better lift-to-drag performance but may be less stable at high speeds.

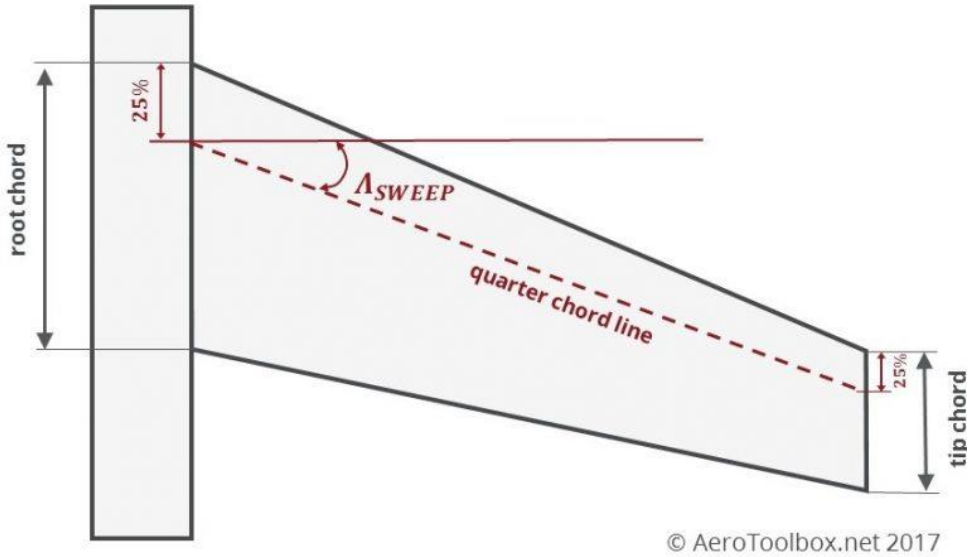

Figure 2.2 Sweep Angle Schematic

The geometry of the wing should have negligible sweep because the aircraft will be operating at low speeds. Sweep will also increase weight and reduce the available solar cell area, both of which will hinder the aircraft's performance.

Therefore sweep angle is taken as 0° for preliminary design UAV.

2.3.2 Wing Area and Aspect Ratio

Wing area is important in determining the lift capacity of an aircraft, while aspect ratio is important in determining its aerodynamic efficiency. A higher aspect ratio wing has a longer, narrower shape that tends to be more efficient at producing lift but may also be more prone to structural instability. A lower aspect ratio wing has a wider, shorter shape that is less efficient at producing lift but provides better maneuverability and structural stability.

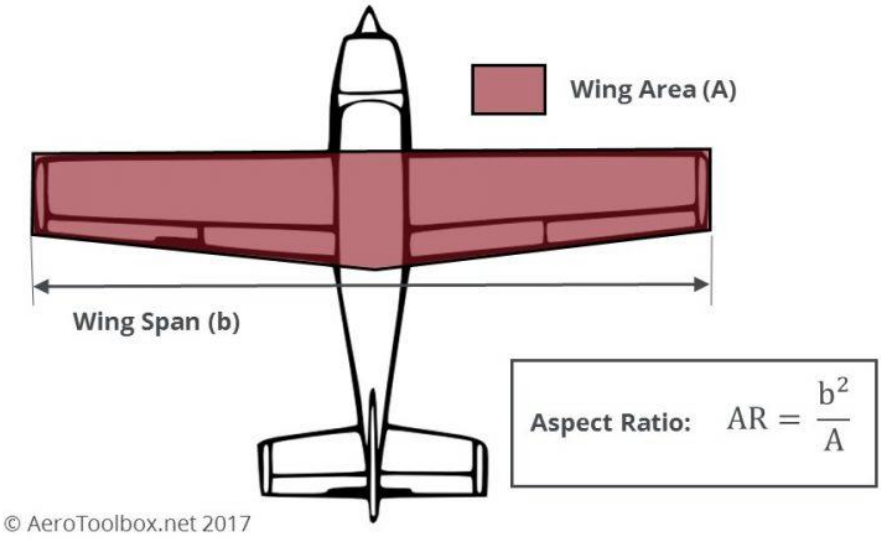

Figure 2.3 Wingspan Schematic

Aspect ratio and Wingspan are taken into consideration as 12 and 8m and wing area can be roughly calculated as follows;

$12 = \frac{8^2}{A}$; hence A = 5.33 m^2 This is the maximum available Wing Area; however it is not possible use whole area to insert Solar Cells.

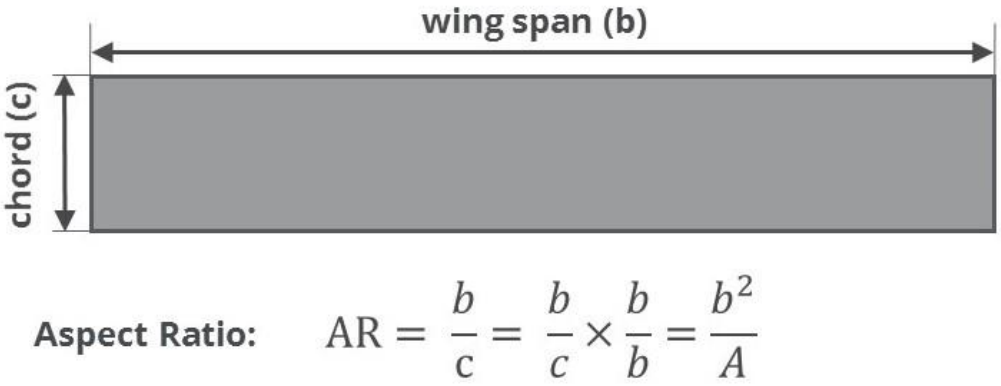

Figure 2.4 Chord Equation

In other words, Aspect ratio is the ratio of the span of the wing to its chord hence [17];

$$A = b \times c\,;\ 5.33\,m^2 = 8\,m \times c \quad (1)$$

c = 0.666 m [chord length]

2.4 Airfoil Selection

2.4.1 Reynold Number determination for Cruise Flight

For this thesis, calculating the appropriate Reynolds number for the Unmanned Air Vehicle (UAV) design is important. The Reynolds number is a dimensionless number that determines the fluid behavior and significantly impacts aerodynamic performance. The appropriate Reynolds number may vary depending on design speed and dimensions. In this case, an appropriate Reynolds number will be calculated for a design speed of 31 m/s, a chord length of 0.666, and a kinematic viscosity of 1.332e-5.

The appropriate Reynolds number can be calculated using the following formula:

$$Re = (\rho * V * c) / \mu \quad (2)$$

Here, ρ represents fluid density, V represents velocity, c represents chord length, and μ represents kinematic viscosity.

From equation 2, Reynolds number becomes 1,549,535.

2.4.2 Analysis and Selection of Airfoils

To select the most appropriate airfoil shape for the design, a detailed analysis was performed using the XFLR5 program, a widely used open-source tool for aerodynamic analysis. This tool provides accurate and reliable results for the aerodynamic characteristics of airfoil shapes under different conditions, making it a suitable choice for this study.

All airfoils selected for the analyses were chosen from open-source libraries and were deemed suitable for Reynolds numbers ranging from 1 million to 2 million, which are relevant to the design specifications of the Unmanned Air Vehicle (UAV). A rigorous selection process was carried out to ensure that all airfoils considered were of high quality and had been validated in previous studies.

The analysis was performed by examining the aerodynamic properties of the airfoils under various operating conditions, such as different angles of attack and Reynolds numbers. Airfoils that did not perform well during simulation and analysis were excluded from the final results presented in the figures below.

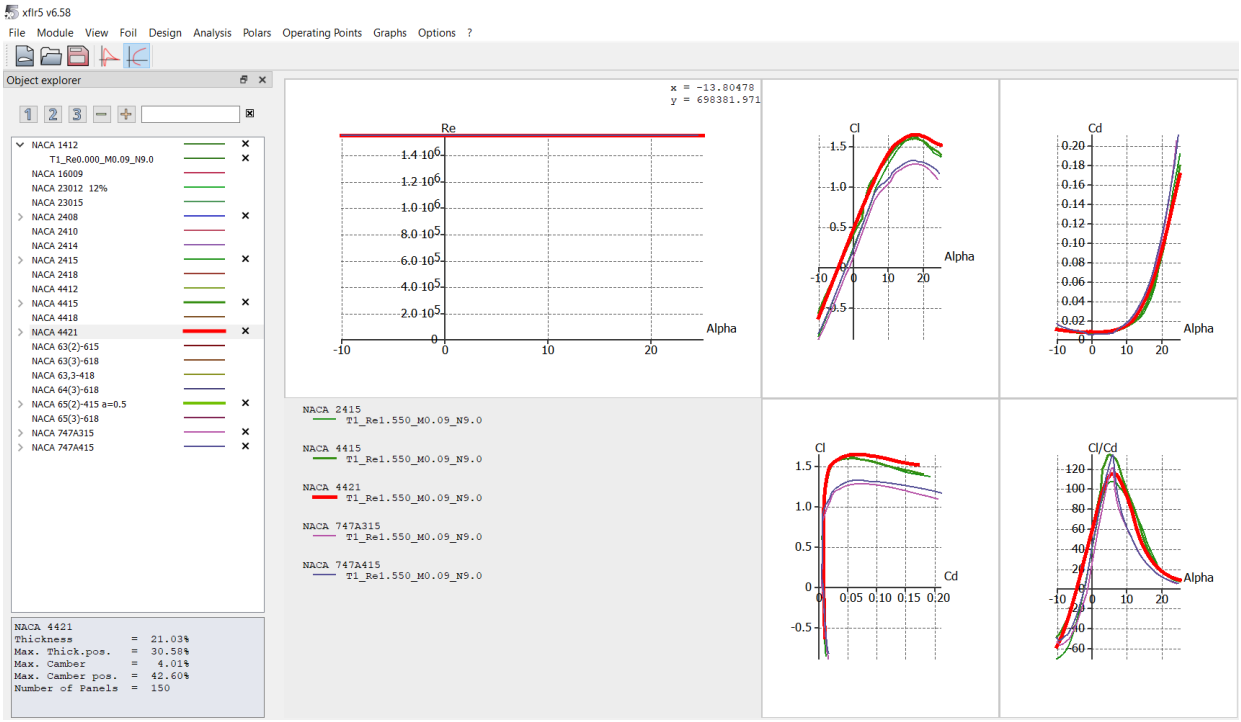

Figure 2.5 Screenshot From Xflr5-1

In these simulation, the aim is to achieve the highest possible coefficient lift (C_L) and the minimum coefficient drag (C_D) values.

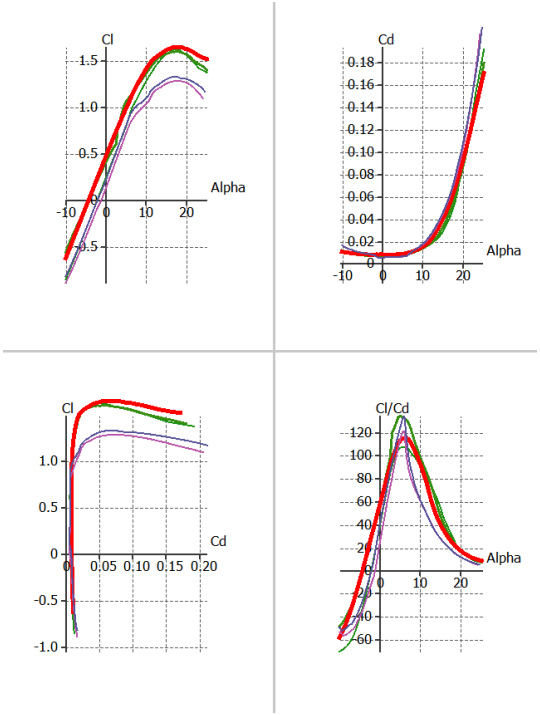

Figure 2.6 Drag and Lift Coefficient Simulation for various Airfoil shape.

As you can see from the study and figure 2.7;the airfoil NACA 4421 seems most suitable for preliminary.

2.4.3 More detailed analysis of NACA 4421

Coefficient of Drag and Lift forces are examined by changing angle of attack angle . All the simulations on the XFLR5 are run from alpha value -10° to 25°.

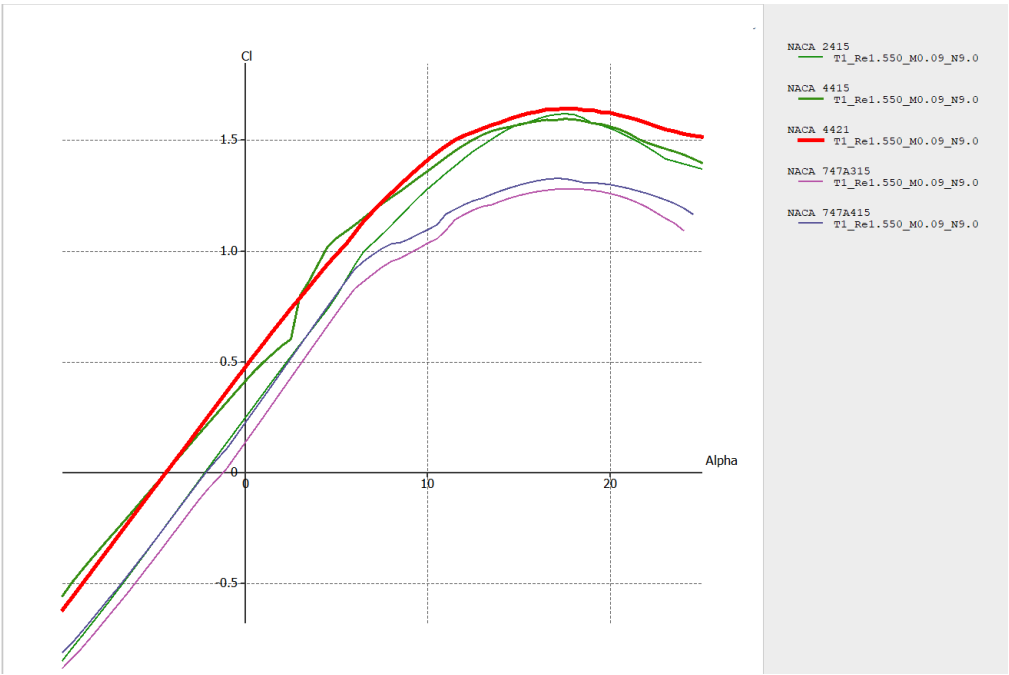

Figure 2.7 Cl vs Alpha

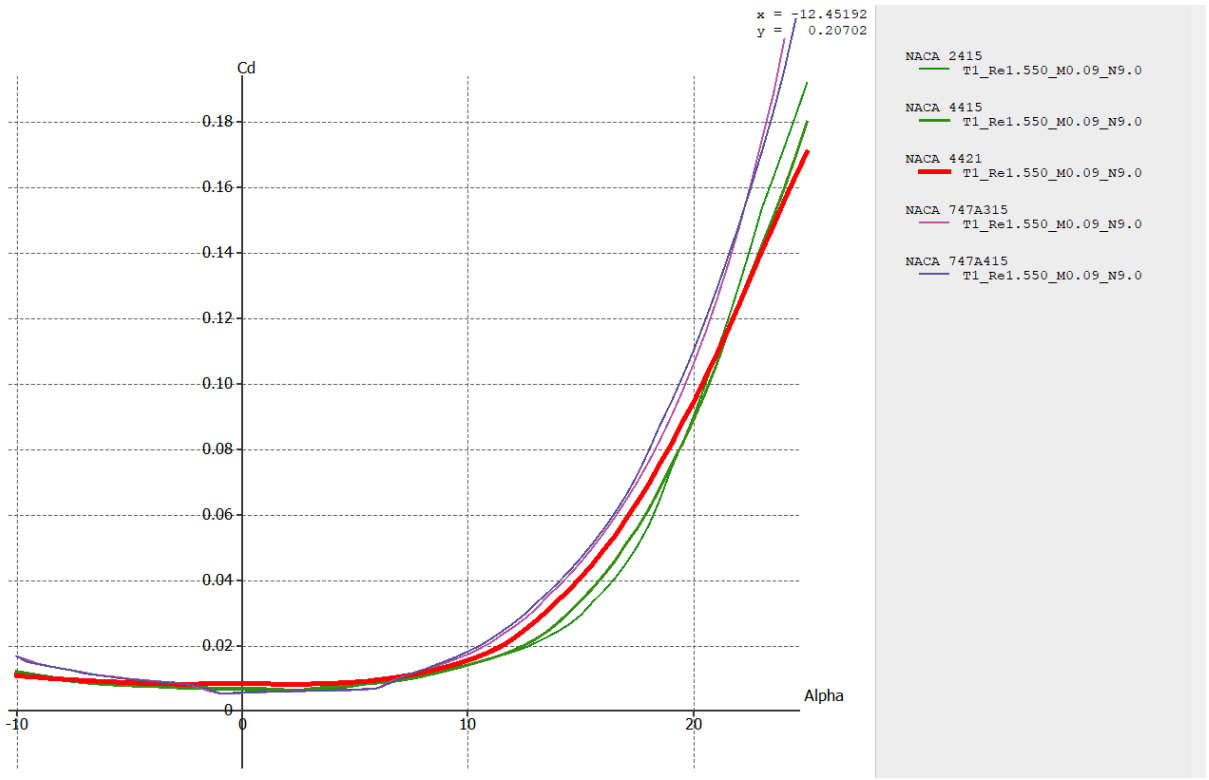

Figure 2.8 Cd vs Alpha

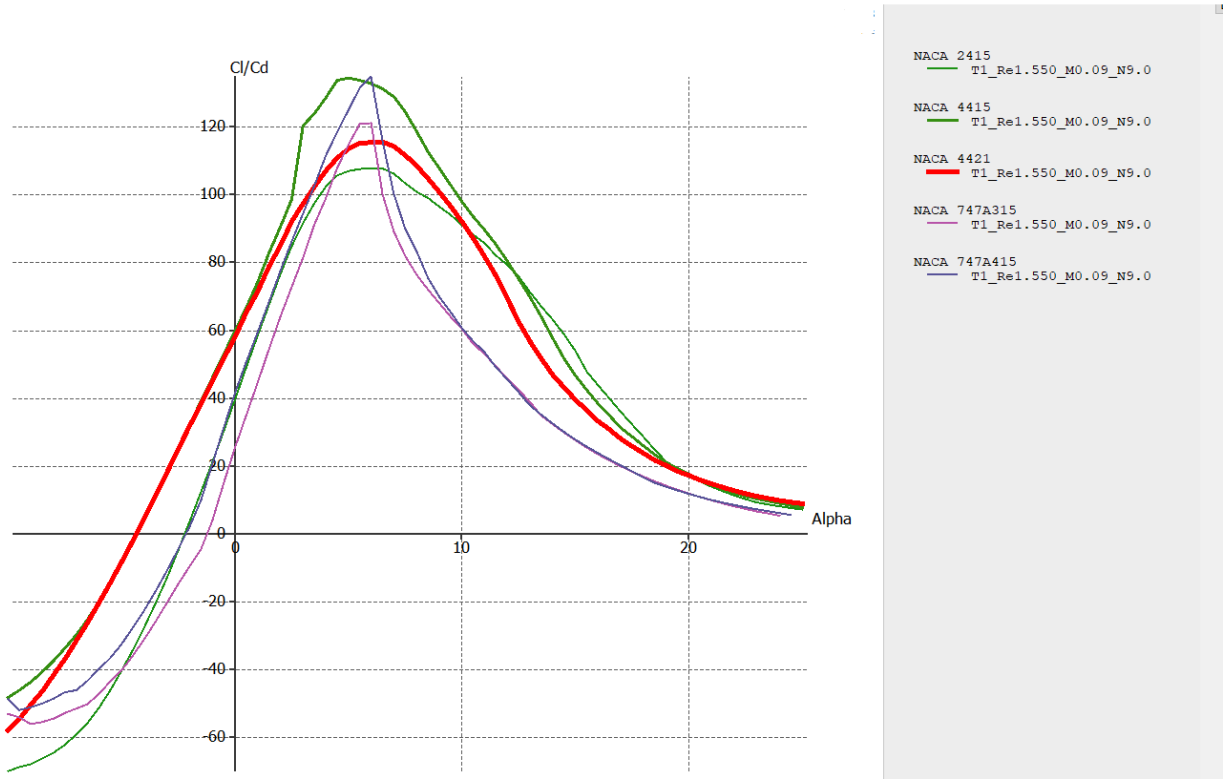

Figure 2.9 Cl/Cd vs Alpha

2.4.4 Detailed View and Specification of Selected Airfoil

Specification of NACA 4421

Max thickness 21% at 30% chord.

Max camber 4% at 40% chord

The NACA 4421 airfoil is a specific aerodynamic profile widely used in aviation and aerodynamics research. Here are the specifications of the NACA 4421 airfoil:

- NACA: The National Advisory Committee for Aeronautics (NACA) developed a standardized numbering system for airfoils, and "4421" is the specific designation for this airfoil.
- Four-digit series: The NACA four-digit series airfoils have a camber line that is defined by a four-digit number, in this case, "4421." The first digit, "4," represents the maximum camber as a percentage of the chord length. In the case of the NACA 4421, the maximum camber is 4% of the chord length.
- Second digit: The second digit, "4," represents the location of the maximum camber as a percentage of the chord length. In the case of the NACA 4421, the maximum camber is located at 40% of the chord length from the leading edge.
- Third and fourth digits: The third and fourth digits, "2" and "1," represent the thickness-to-chord ratio as a percentage. In the case of the NACA 4421, the airfoil has a thickness-to-chord ratio of 21%.

Overall, the NACA 4421 airfoil is characterized by its 4% camber, located at 40% of the chord length, and a thickness-to-chord ratio of 21%. These specifications determine the aerodynamic properties of the airfoil and its performance characteristics in various applications, such as aircraft wings, wind turbines, and hydrofoil designs.

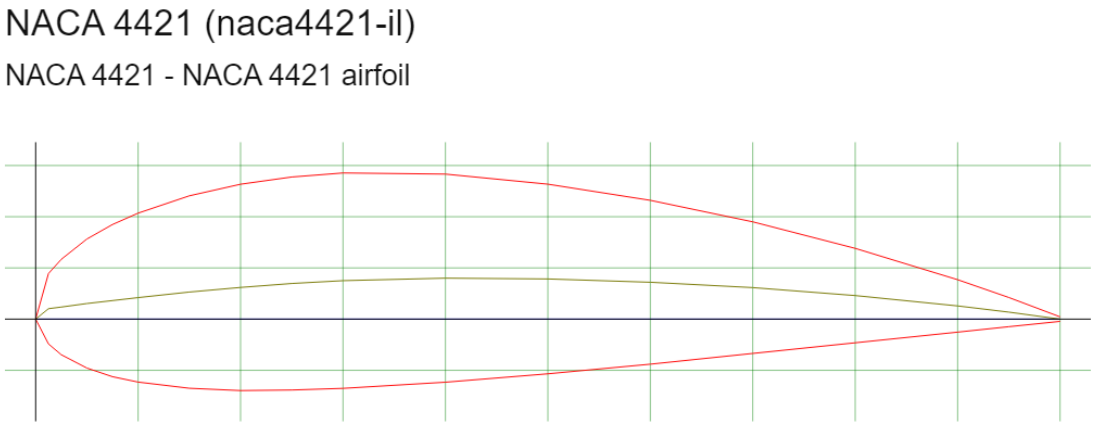

Figure 2.10 NACA 4421 2D view

2.4.5 3D view, Force & Pressure Distribution on Wing (XFLR 5)

All analyses were conducted for a cruise speed of 31 m/s, a Reynolds number of 1.5 million, and an altitude of 3000 feet. These specific parameters were chosen to study the aerodynamic performance of the system under realistic operating conditions.

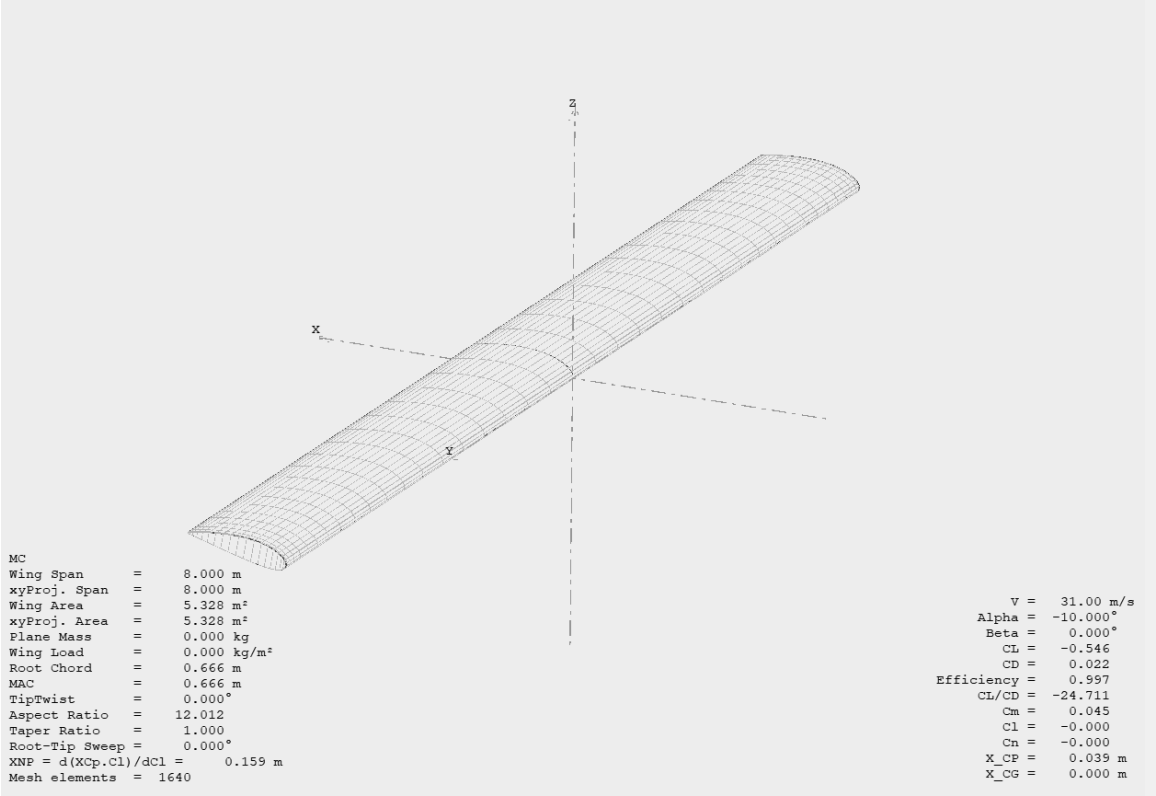

Figure 2.11 Meshes on Wing @ XFLR5

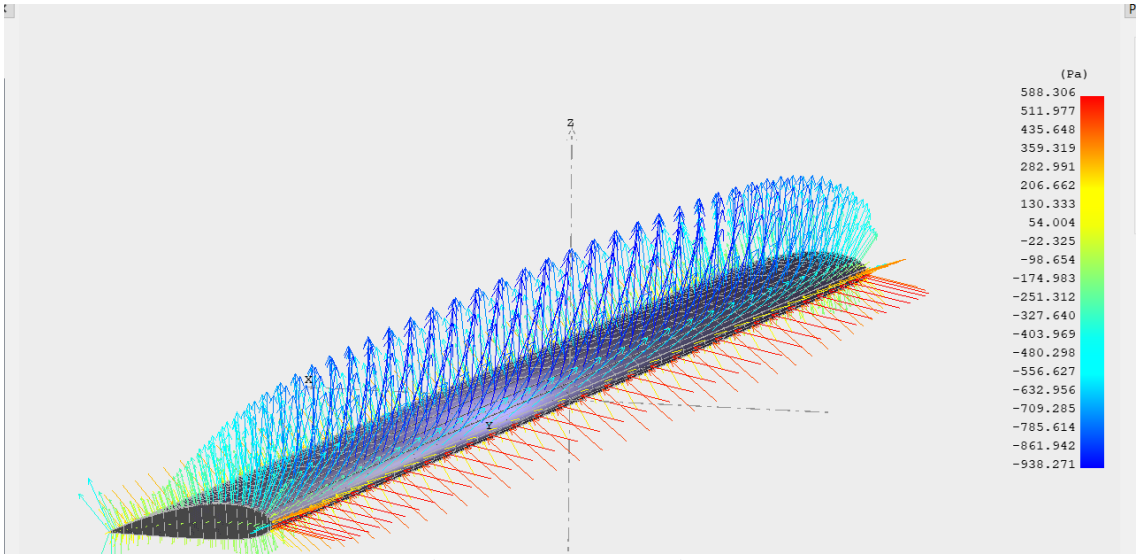

Figure 2.12 Pressure on Wing

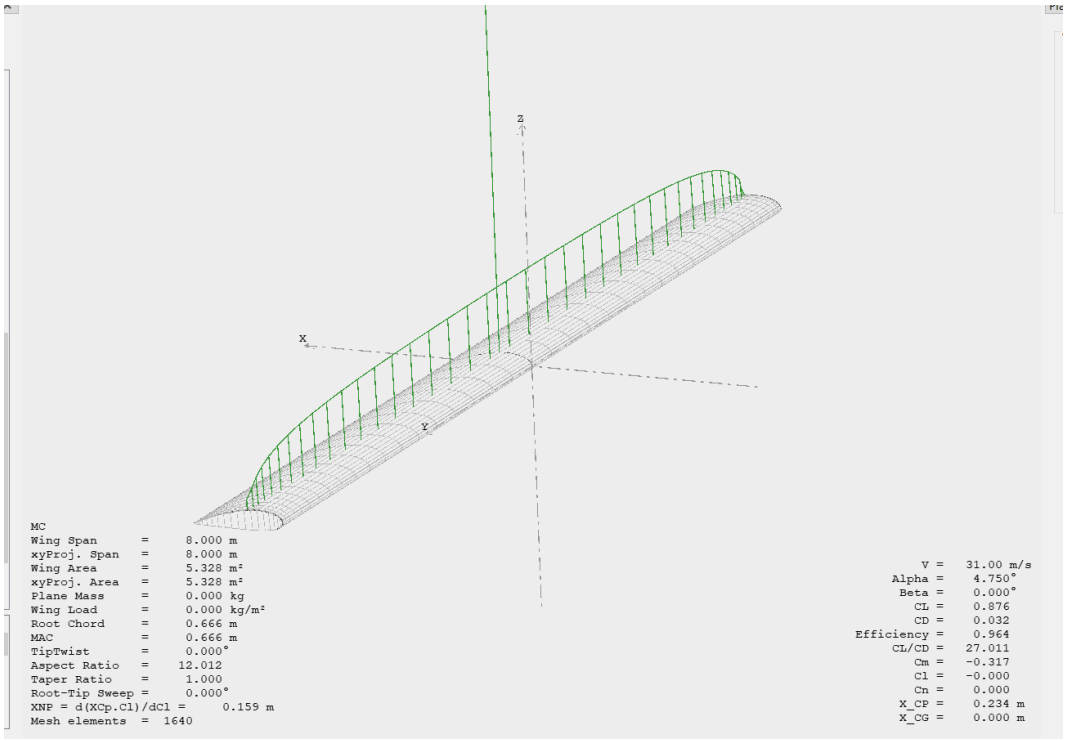

Figure 2.13 Lift Forces @4.75-degree angle of attack

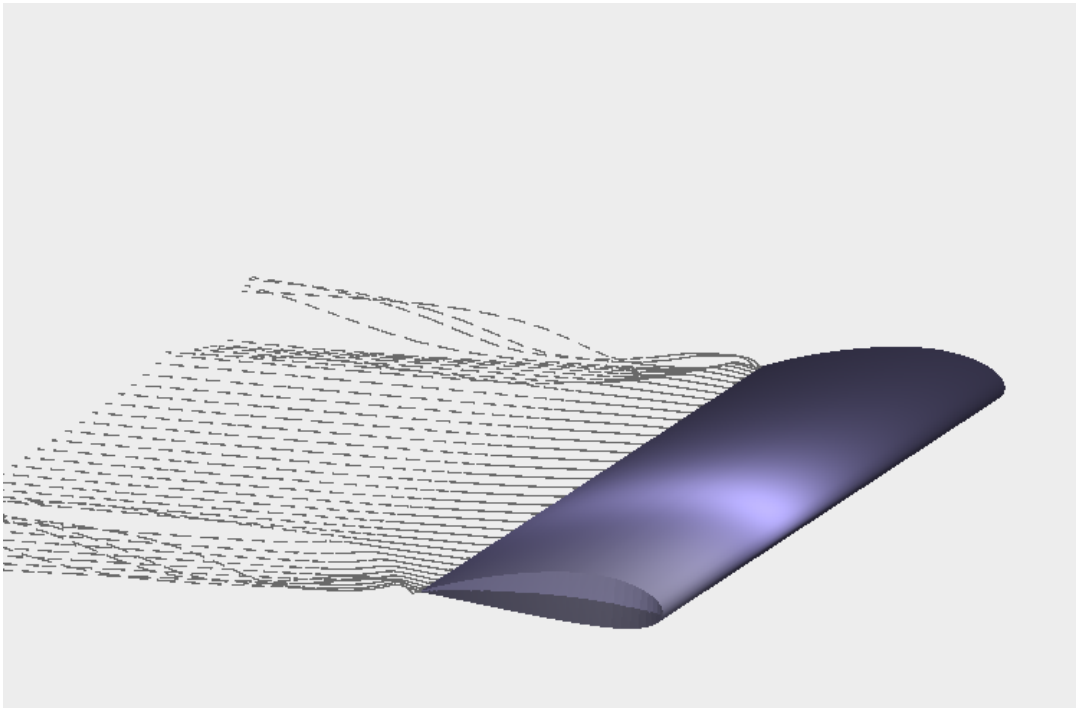

Figure 2.14 Stream View

2.5 Solar Cell Selection

2.5.1 Gallium Arsenide

Gallium arsenide (GaAs) solar cells are widely used in various applications due to their high efficiency and excellent radiation resistance. GaAs solar cells are commonly used in space applications, such as satellites, due to their ability to generate electricity efficiently even in low light conditions. They are also used in aviation, particularly in unmanned air vehicles (UAVs) and other aerospace systems that require high performance and reliability.

In space applications, GaAs solar cells have a long history of use and have been extensively studied and tested. The excellent radiation resistance of GaAs makes it an ideal material for use in space, where exposure to harsh radiation environments can cause significant degradation in the performance of other solar cell materials. The use of GaAs solar cells has contributed to the success of many space missions, including the Hubble Space Telescope and the Mars Exploration Rovers.

In aviation, GaAs solar cells are particularly suited for use in UAVs due to their high-power density, lightweight and compact design. UAVs require reliable and efficient power sources to operate effectively in remote locations, and GaAs solar cells provide a solution for this requirement. In addition to UAVs, GaAs solar cells are also used in other aerospace systems, such as high-altitude aircraft and drones. The high efficiency and radiation resistance of GaAs solar cells make them a preferred choice in these applications where performance and reliability are critical.

2.5.2 Selection of proper Commercial GaAs Solar cell

The research conducted on GaAs solar cells through multiple companies is a crucial step in determining the most efficient solar cell for a particular application. By analyzing data sheets from different manufacturers, researchers can compare the performance characteristics of different solar cells, including efficiency, power output, and durability. In this case, the decision to use data from a commercial GaAs solar cell with a 32% efficiency is likely the result of careful analysis and consideration of multiple factors, including cost, performance, and availability.

Overall, GaAs solar cells represent an important advancement in the field of photovoltaics, offering high efficiency and unique characteristics that make them well-suited for certain applications. As research continues, it is likely that we will see further improvements and refinements in GaAs solar cell technology, leading to even more efficient and cost-effective solutions for generating clean energy from sunlight.

While the data sheet of the referenced commercial solar cell indicated its suitability in terms of efficiency, it did not explicitly mention its flexibility. [18]. As a result, an alternative commercial product with a 29.5% efficiency was proposed, considering the aspect of flexibility. [19].

2.6 Integration of Solar Cell onto UAV wing

Along with the array lamination and circuit formation, the cells were soldered together to form the sized array. soldering was mainly based on the usage of tin tabbing strips for its high electrical conductivity and availability. The subsequent figures are shots of the actual lamination operation.

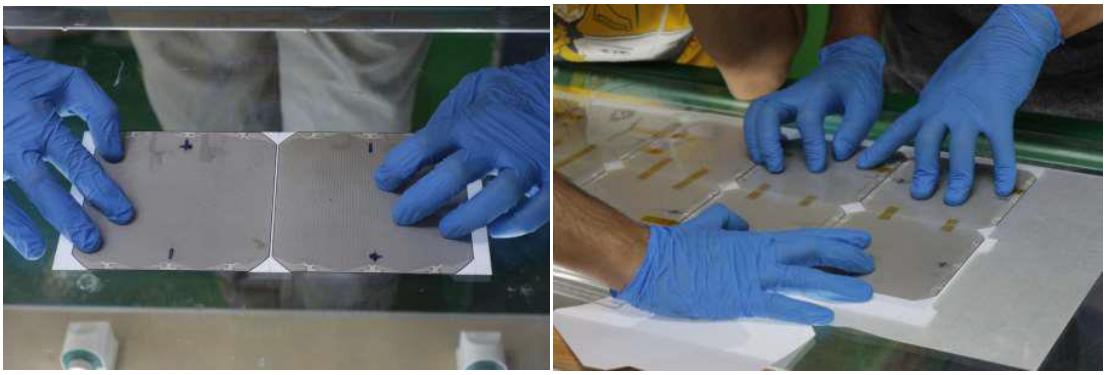

Figure 2.15 Integration of Solar Cells

In addition to the lamination process and circuit formation, the solar cells were interconnected by soldering to create the desired array size. Soldering was performed using tin tabbing strips due to their high electrical conductivity and widespread availability. The following images depict the actual lamination process.

To ensure a secure and reliable integration of solar cells onto the UAV wing, a specialized adhesive was applied. This adhesive provided a strong bond between the cells and the wing surface, ensuring proper alignment and stability. The integration process involved carefully positioning the solar cells onto the wing, considering factors such as aerodynamic considerations and optimal sunlight exposure.

Once the solar cells were securely attached, additional layers of protective coating were applied to enhance durability and weather resistance. These coatings acted as a barrier against environmental factors such as moisture, UV radiation, and temperature fluctuations, safeguarding the solar cells and prolonging their lifespan.

The integration of solar cells onto the UAV wing was conducted with utmost precision and attention to detail. Stringent quality control measures were implemented to verify the integrity and performance of each cell and the overall array. This integration process played a crucial role in maximizing the energy-harvesting capabilities of the UAV and ensuring its efficient and sustainable operation.

The airfoil is extruded on SolidWorks with 8 meters wingspan as below.

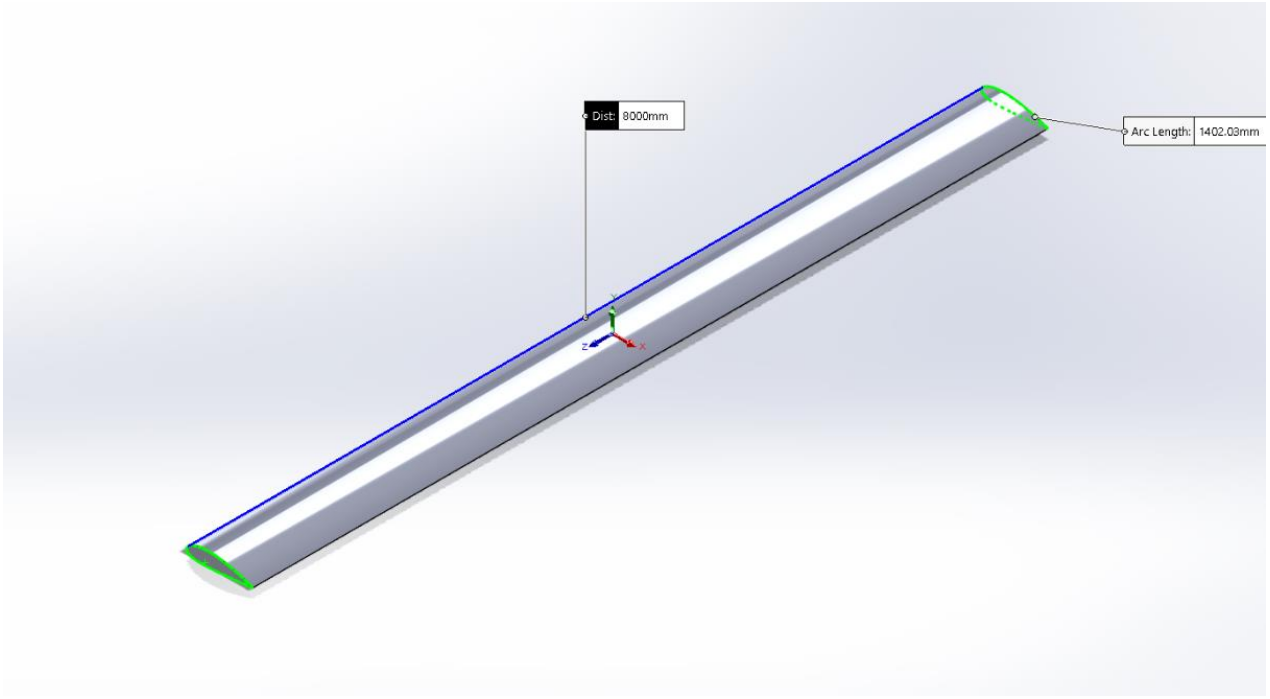

Figure 2.16 Wing 3D Model

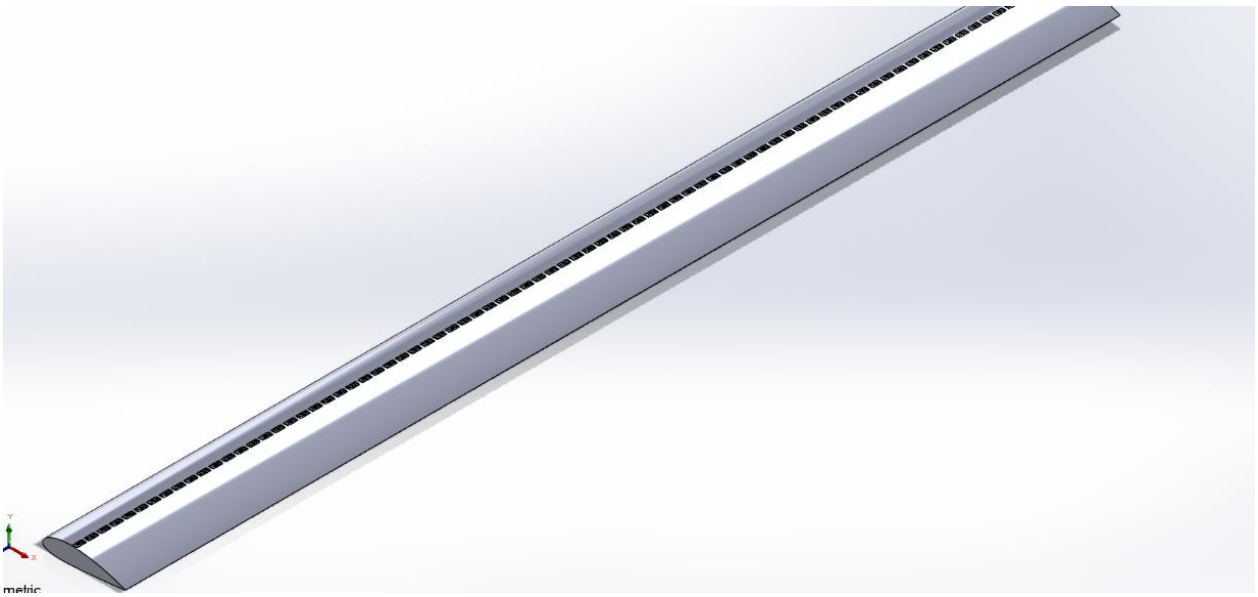

Figure 2.17 Solar cells before pattern operation

The integration of solar cells onto the UAV wing was carefully planned and executed using SolidWorks software. SolidWorks allowed for precise placement and alignment of the solar cells on the wing surface.

First, the dimensions and shape of the solar cells were imported into SolidWorks. Engineers then designed the layout and placement of the cells on the wing, considering factors such as maximum exposure to sunlight and minimal interference with the aerodynamics of the UAV.

Using SolidWorks' assembly features, the solar cells were positioned and oriented accurately on the wing surface. The software provided tools for aligning and spacing the cells evenly, ensuring uniform coverage and efficient utilization of the available space.

Additionally, SolidWorks allowed engineers to simulate the integration process, visualizing how the solar cells would fit and interact with the wing structure. This enabled them to identify any potential issues or conflicts and make necessary adjustments before proceeding with the physical integration.

By leveraging SolidWorks' capabilities for precise placement and simulation, the integration of solar cells onto the UAV wing was executed with precision and efficiency. This ensured optimal utilization of solar energy and contributed to the overall performance and endurance of the UAV during flight.

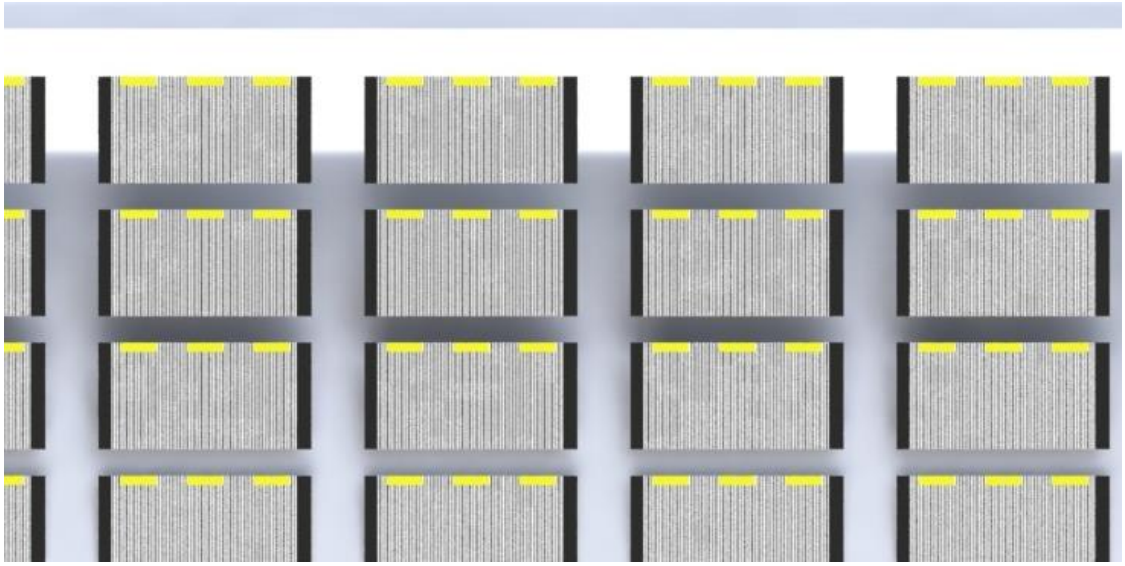

Figure 2.18 Solar cells rendered view.

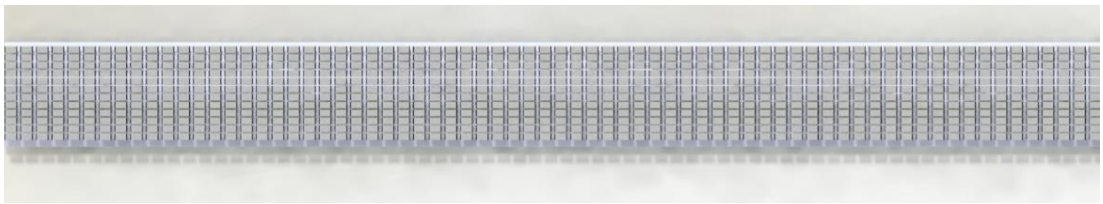

Figure 2.19 Rendered view of Solar Cell Integrated Wing

The available solar cell area depends on several factors such as the power required by the UAV, the efficiency of the solar cells, and the wing area. To determine the required solar cell area, the power consumption of the UAV should be calculated. Then, the required solar cell area can be estimated by considering the efficiency of the solar cells and the solar irradiance in the operating environment.

It is also important to consider the weight and aerodynamic impact of the solar cells on the wing. The solar cells should not add excessive weight to the UAV or create additional drag. Therefore, the solar cell area should be optimized to provide the required power while minimizing weight and drag.

In addition, the integration of solar cells onto the wing should be carefully designed to ensure proper airflow over the wing surface. The solar cells should not disrupt the airflow and cause turbulence, which can negatively impact the performance and stability of the UAV. Therefore, the solar cell placement and orientation should be optimized to ensure smooth airflow over the wing surface.

Several methods can be used to integrate solar cells into the wing. In this project, a sandwich structure will be used, with a thin layer of solar cells being inserted between two layers of composite materials. The solar cells will be placed on the top surface of the wing to ensure maximum exposure to sunlight. This integration method not only reduces weight but also enhances the wing's structural integrity and aerodynamic performance. The sandwich structure will also protect the solar cells from any potential damage caused by wind or other environmental factors.

For the preliminary design, the gap between the solar cells was assumed to be 5 mm along the longitudinal edge (x-axis) and 2 mm along the width (y-axis). In this case, the total area of the solar cells was calculated to be 4.1552 m^2, and it was determined that a total of 1484 (106x14) solar cells could be used.

In the designed profile, the area for one solar cell is 0.0028 m^2 (40 mm * 70 mm). The panels are placed on the wing with 14 panels along the y-axis and 106 panels along the x-axis, totaling 1484 panels. Therefore, the total area covered by solar cells is calculated as 4.1552 m2, which represents approximately 77.95% of the total wing area.

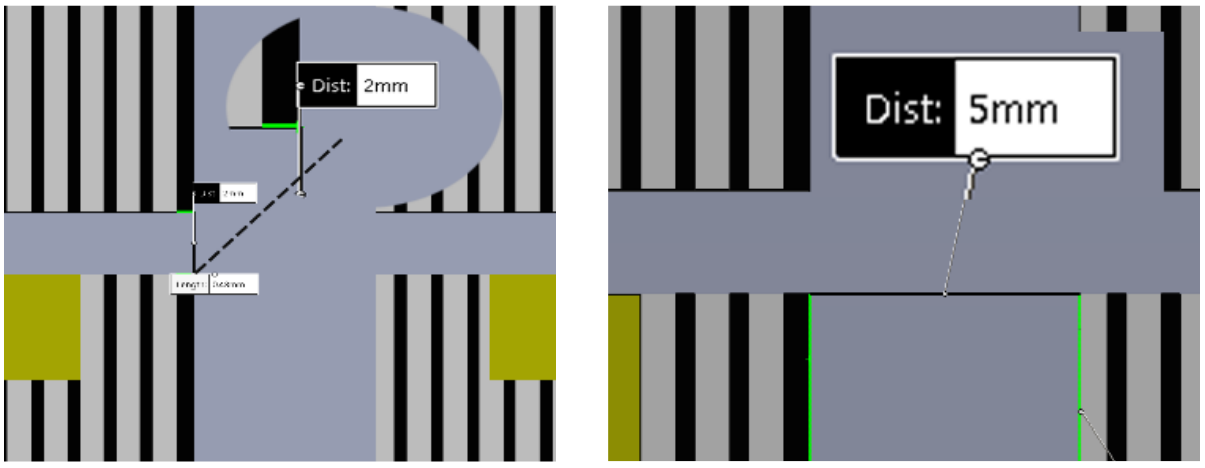

Figure 2.20 Spacing of Solar Cell Along y and x axis.

3 CALCULATIONS AND RESULTS

3.1 Determination of Power Available and Daily Electrical Energy Required

For UAV design, it is assumed that it is at steady level flight. At steady level flight, the lift force generated by the wing exactly compensates for the weight and the propeller thrust compensates for the drag force. Using following equations

$$W = mg = C_L \frac{\rho}{2} S V^2 \qquad (3)$$

$$T = D = C_D \frac{\rho}{2} S V^2 \qquad (4)$$

We can conclude that the level flight speed must be:

$$V = \sqrt{\frac{2mg}{C_L \rho S}} \qquad (5)$$

And then substitute it in equation [4] in order to calculate the power for level flight.

$$P_{req} = \frac{C_D}{C_L^{\frac{3}{2}}} \sqrt{\frac{(mg)^3}{S}} \sqrt{\frac{2}{\rho}} \qquad (6)$$

Using the definition of aspect ratio AR; rewrite the previous equation where b is the wingspan;

$$P_{req} = T \times V = \frac{C_D}{C_L^{\frac{3}{2}}} \sqrt{\frac{2ARg^3}{\rho}} \frac{m^{3/2}}{b} \qquad (7)$$

Equation [7] gives the power required for steady level flight.

To calculate the daily required electrical energy that the UAV must use for steady level flight;

$$P_{Daily,Total} = \frac{1}{n_{ctrl} n_{mot} n_{grb} n_{plr}} P_{req} + \frac{1}{n_{bec}} (P_{av} + P_{pld}) \qquad (8)$$

Equation [3] through [8] will be used for the weight analysis of some components for the UAV.

Where;

- η_{ctrl} is the motor controller efficiency
- η_{mot} is the motor efficiency
- η_{prop} is the propeller efficiency
- η_{bec} is the battery eliminator circuit (step-down) efficiency
- $\eta_{battdischg}$ is the battery discharging efficiency
- $\eta_{spdctrl}$ is the speed controller efficiency
- P_{other} is the power drain from other electronics

Angle of attack shall be considered as 2°-3° for cruise conditions, hence from figure 2.8 and 2.9 ; lift and drag coefficients are taken as C_D=0.01,C_L=0.7 .

In addition, the service altitude of UAV shall be 3 000 feet. By using this information density of air at 3000 feet is

Physical Properties of U.S. Standard Atmosphere, 1976 in SI Units				
Altitude (meters)	**Temperature (K)**	**Pressure (Pa)**	**Density (kg/m^3)**	**Viscosity (N-s/m^2)**
-2,000	301.15	1.27774E+5	1.47808	1.87630E-5
-1,000	294.65	1.13929E+5	1.34700	1.84434E-5
0	288.15	1.01325E+5	1.22500	1.81206E-5
1,000	281.65	8.98746E+4	1.11164	1.77943E-5
2,000	275.15	7.94952E+4	1.00649	1.74645E-5
3,000	268.65	7.01085E+4	9.09122E-1	1.71311E-5
4,000	262.15	6.16402E+4	8.19129E-1	1.67940E-5
5,000	255.65	5.40199E+4	7.36116E-1	1.64531E-5
6,000	249.15	4.71810E+4	6.59697E-1	1.61084E-5
7,000	242.65	4.10607E+4	5.89501E-1	1.57596E-5
8,000	236.15	3.55998E+4	5.25168E-1	1.54068E-5
9,000	229.65	3.07425E+4	4.66348E-1	1.50498E-5
10,000	223.15	2.64363E+4	4.12707E-1	1.46884E-5
12,000	216.65	1.93304E+4	3.10828E-1	1.43226E-5
15,000	216.65	1.20446E+4	1.93674E-1	1.43226E-5
20,000	216.65	5.47489E+3	8.80349E-2	1.43226E-5
25,000	221.65	2.51102E+3	3.94658E-2	1.46044E-5
30,000	226.65	1.17187E+3	1.80119E-2	1.48835E-5
35,000	237.05	5.58924E+2	8.21392E-3	1.54559E-5
40,000	251.05	2.77522E+2	3.85101E-3	1.62096E-5
45,000	265.05	1.43135E+2	1.88129E-3	1.69449E-5
50,000	270.65	7.59448E+1	9.77525E-4	1.72341E-5
60,000	245.45	2.03143E+1	2.88321E-4	1.59104E-5
70,000	217.45	4.63422	7.42430E-5	1.43679E-5
80,000	196.65	8.86280E-1	1.57005E-5	1.31682E-5
84,852	186.95	3.73384E-1	6.95788E-6	1.25915E-5

Basic Assumptions

Air is a clean, dry, perfect gas mixture; Specific heat ratio = 1.40; Molecular weight to 86 km = 28.9644
Principal sea-level constituents: N_2–78.084%, O_2–20.9476%, Ar–0.934%, CO_2–0.0314%, Ne–0.001818%, He–0.000524%, CH_4–0.0002%

Table 3 Physical Properties U.S. Standard Atmosphere

$\rho_{air} = 1.111$ kg/m3 @3000 feet (3000 feet =914,4 meters)

Cruise speed is also given as V_{cruise}= 31 m/s by the supporting company.

Mass of UAV is taken as 200 kg by the supporting company.

From equation (6)

$$P_{req} = T \times V = \frac{C_D}{C_L^{\frac{3}{2}}}\sqrt{\frac{(mg)^3}{S}}\sqrt{\frac{2}{\rho}} = \frac{0.1}{0.7^{\frac{3}{2}}}\sqrt{\frac{(200kg*9.81\ m/s^2)^3}{5{,}33\ m^2}}\sqrt{\frac{2}{1.111\ kg/m^3}}$$

$$P_{req} \approx 825 \text{ Watt}$$

3.2 Solar Energy Calculations

Solar energy collection and energy management is very critical for the performance and endurance of solar powered UAV's. As the UAV is being designed to have longer endurance and lower cost operations, solar power system must be designed as to reach optimum point. Solar irradiation calculation is an important part of any solar energy collection process. Using these calculations for a mobile aircraft over its mission course requires assumptions and simplified models.

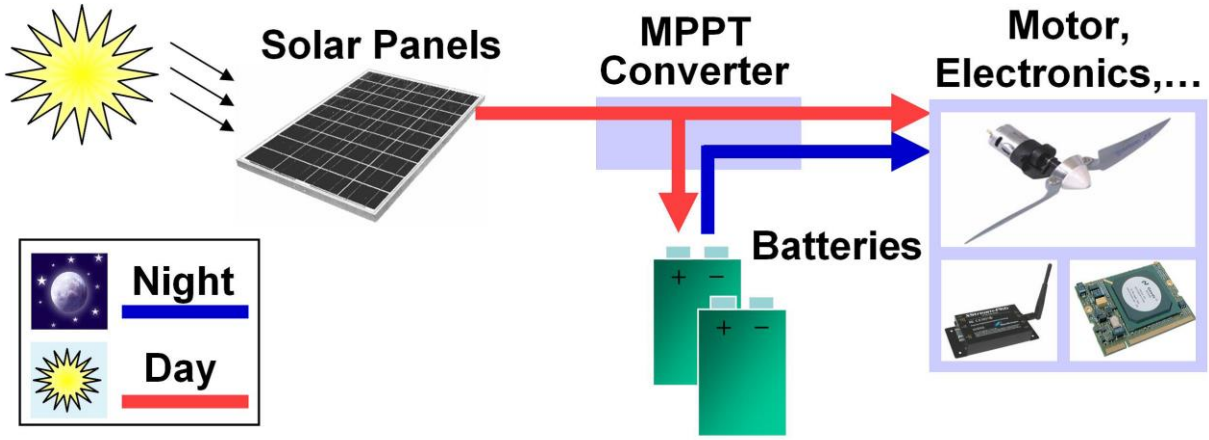

Figure 3.1Power system of solar powered UAV

As you can see from figure 3.1 the solar cells supply voltage and current to MPPT. Then MPPT converts this voltage and current so that it efficiently matches recharging voltage of the batteries and current draw by avionics on board. Therefore, power available will be calculated according to the solar power acquired from solar cells, efficiency of MPPT (Maximum Power Point Tracking), ESC(Electronic Speed Controllers) and propulsion unit (motor and propeller).

Total radiation is the sum of beam radiation and diffuse radiation. Beam radiation is due to the solar light rays hitting directly on the PV panels. Diffuse radiation
is due to reflected or refracted light rays because of atmospheric obstacles (clouds
etc.). We assumed it is a cloudless day so the beam radiation will be almost equal to the total radiation, leaving the diffuse radiation almost equal to zero.
Therefore, the diffuse radiation component of the total radiation will be ignored.

For the reach optimum power available calculations incoming solar irradiation estimation should be done for the specific dates of flight.

3.2.1 SOLAR IRRADIATION ESTIMATION

For calculations the hourly integrated solar irradiation formula will be used;

$$I_0 = \frac{12*3600}{\pi} G_{sc} \left(1 + 0.033 \cos \frac{360n}{365}\right) * [(\cos\phi \cos\delta (sin\omega_2 - \omega_1) + \frac{\pi(\omega_2 - \omega_1)}{180} \sin\phi \sin\delta] \quad (9)$$

θ :**Angle of incidence**, the angle between the beam radiation on a surface and the normal to that surface.

G_{sc}: **Solar constant**= 1367 W/m^2

δ: **Declination** can be found from the table below.

n: **Day number** can be found using table below

Month	n for ith Day of Month	For Average Day of Month		
		Date	n	δ
January	i	17	17	−20.9
February	$31 + i$	16	47	−13.0
March	$59 + i$	16	75	−2.4
April	$90 + i$	15	105	9.4
May	$120 + i$	15	135	18.8
June	$151 + i$	11	162	23.1
July	$181 + i$	17	198	21.2
August	$212 + i$	16	228	13.5
September	$243 + i$	15	258	2.2
October	$273 + i$	15	288	−9.6
November	$304 + i$	14	318	−18.9
December	$334 + i$	10	344	−23.0

[a]From Klein (1977). Do not use for $|\phi| > 66.5°$.

Figure 3.2 Solar Angle Table

ϕ: **Latitude of the position of the UAV** (location) 37^{o} .

R_b: **Geometric factor** will also be used if there different alignments of solar panels

$$R_b = \frac{cos\theta}{cos\theta_z} \quad (10)$$

$$cos\theta = \sin\delta \sin(\phi - \beta) + \cos\delta \cos(\phi - \beta) \cos\omega \quad (11)$$

$$cos\theta_z = \sin\delta \sin\phi + \cos\delta \cos\phi \cos\omega \quad (12)$$

$$I_{est} = I_0 \times R_b \quad (13)$$

$$Energy\ Produced = I_{est} \times Area\ \times \eta_{cell} \quad (14)$$

This equation represents the energy produced; by using total area covered by solar panels with a certain efficiency (ηcell).

Solar power can be calculated as.

$$P_{sol} = S_{total}\, \eta_{sol}(I_{est}) \quad (15)$$

$$\delta = 23.45 \times \sin(360 \times \frac{284+n}{365}) \quad (16)$$

N: **Number of daylight hours** can be calculated by using equation 17.

$$N = \frac{2}{15} \times \cos^{-1}(-\tan(\phi) \times \tan(\delta)) \quad (17)$$

ω :**Hour angle**, Time of the day converted to degrees (12:00 being 0 and for each hour 15 degrees is added or subtracted) can be calculated using equation 18.

$$\omega = 15 \times (local\ time - 12) \quad (18)$$

The symbol (β) used in the equation represents the tilt angle of the panel with respect to the ground. The following diagram illustrates how the tilt angles (β) are determined for the panels:

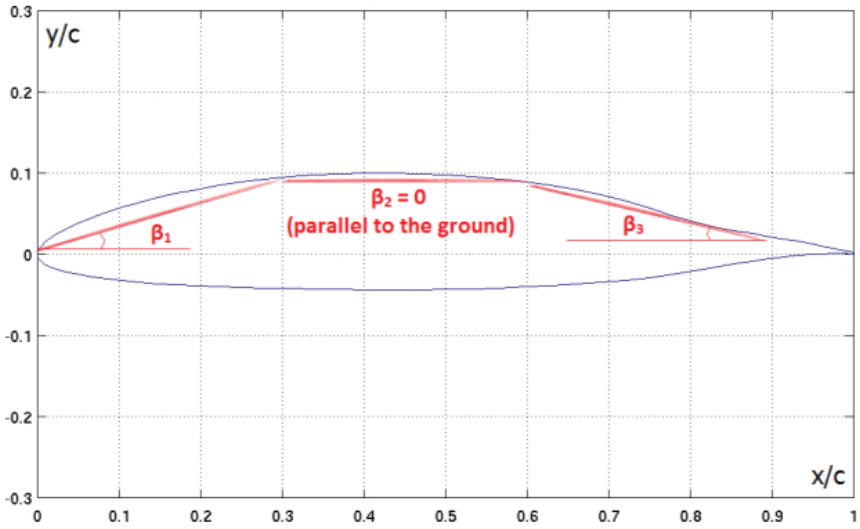

Figure 3.3 Schematic view of Beta angle [22]

Once the panel placement is complete, we obtained the tilt angles (β) by determining the angles between the panels and the ground (horizontal). Since there are 14 rows of panels, we obtained a total of 14 Beta angles. You can see them in the figure below:

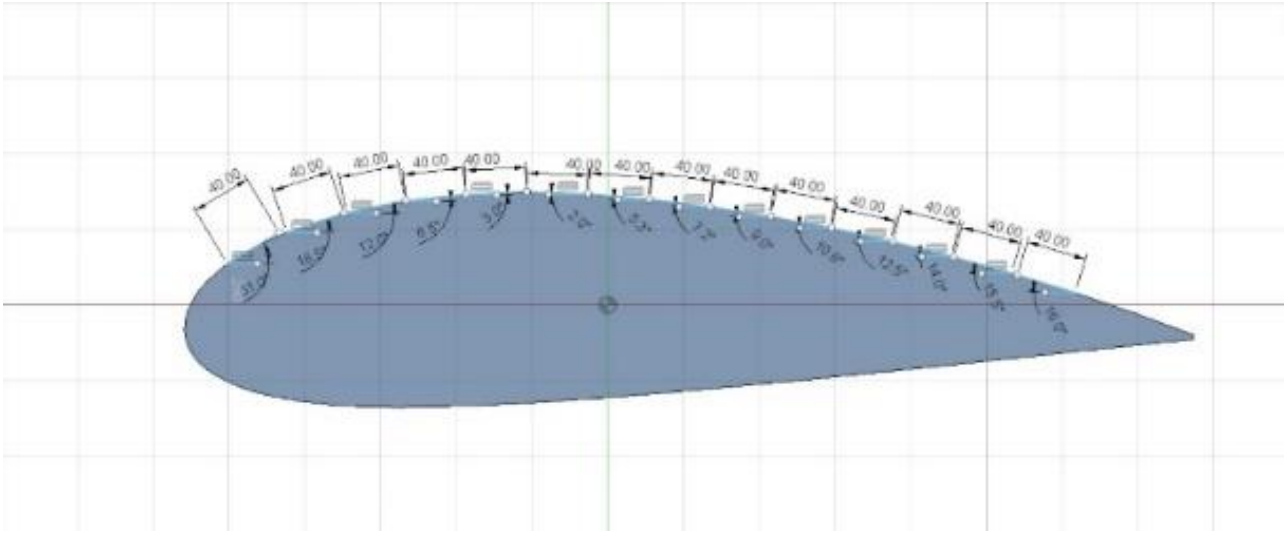

Figure 3.4 Beta Angle on the Airfoil Profile

It is known that the shortest day is the winter solstice, and the longest day is the summer solstice. Using a MATLAB code, the amount of sunshine for the study area has been calculated based on the days of the year, and the obtained values are shown in Figure 3.5

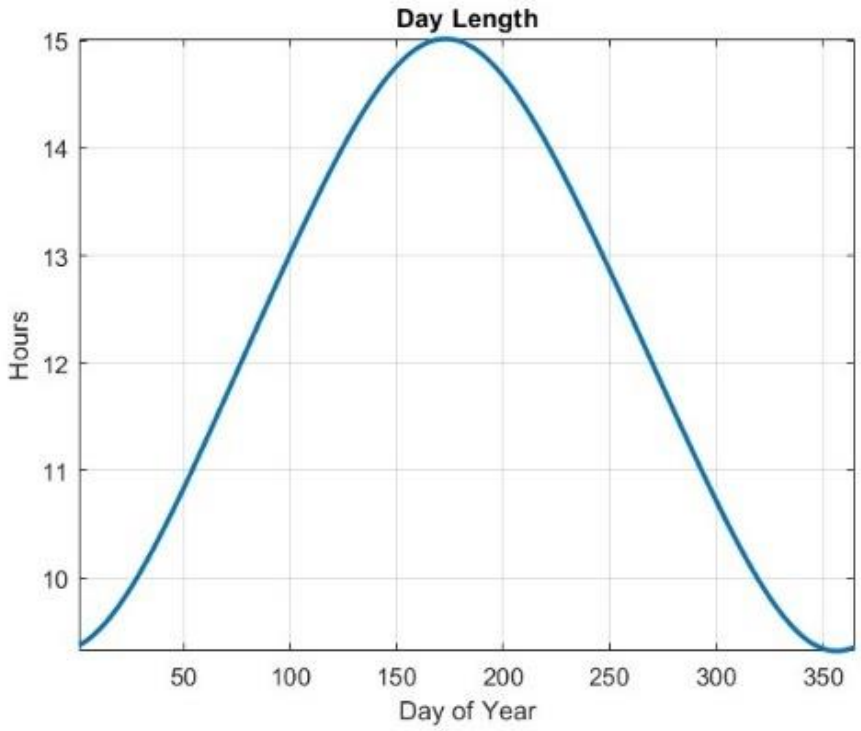

Figure 3.5 The annual duration of daylight for the given latitude value

As can be seen from the figure 3.5 , the longest day occurs on June 21st, which is the 172nd day of the year. Similarly, as read from the same graph, December 21st is the shortest day and the 355th day of the year.

- **For June 21st**

For sunset and sunrise, we calculated from equation 17 also we looked Earth System Research Laboratories [20] to obtain exact hours. On June 21st sunrise occurs at 05:15 and sunset occurs at 19:45.

To obtain acquired energy between hours 05:15 and 19:45. Hour angles calculated using equation 18. Local time decimal must be written by 100's order For example 5:15 local time =5.25 in equation

$$\omega_1 = 15 \times (5.25 - 12) = -101.25$$
$$\omega_2 = 15 \times (19.75 - 12) = 116.25$$

At below shown the calculations for one of our Beta angles $\beta = 12^{o}$ as a representative

$cos\theta = -0.495$

$cos\theta_z = -0.346$

$R_b = 1.429$

$\delta = \text{June 21st} = 23.45^{o}$

$$n = 172$$

$G_{sc} = 1367 \frac{W}{m^2}$

$\phi = 37^o$

When we entered this values in equation 10. Our result is

$I_0 = 4.155 \times 10^7 \frac{J}{m^2}$

This value gives the solar energy falling on the horizontal surface throughout the day. When we multiply this by R_b, we get the solar energy falling on the panel standing at that Beta angle.

$I_{est} = I_0 \times R_b = 4.155 \times 10^7 \times 1.429 = 5.975 \times 10^7 \frac{J}{m^2}$

And finally, we multiply this result with panel efficiency and total area of panel for that beta angle. Then we reach our acquired energy for this certain beta angle.

We already know we have 106 panel for a line.

1 panel area=$0.0028\ m^2$

$total\ panel\ area$ =1 panel area× 106=$0.2968\ m^2$

η_{cell}=Panel efficiency =%29.5

$Acquired\ energy = I_{est} \times total\ panel\ area\ \times \eta_{cell} = 5.232 \times 10^6$ J

When I repeat this process for all beta angles and add up the energies obtained is

$E_{total} = 5.248 \times 10^7\ J = 52\ MJ$

- **For December 21st**

For sunset and sunrise, we calculated from equation 17 also we looked Earth System Research Laboratories [20] to obtain exact hours. On June 21st sunrise occurs at 07:30 and sunset occurs at 17:15.

To obtain acquired energy between hours 07:30 and 17:15. Hour angles calculated using equation 18. Local time decimal must be written by 100's order For example 7:30 local time =7.50 in equation

$$\omega_1 = 15 \times (7.50 - 12) = -67.50$$
$$\omega_2 = 15 \times (17.25 - 12) = 78.75$$

At below shown the calculations for one of our Beta angles $\beta = 12^o$ as a representative

$cos\theta = -0.859$
$cos\theta_z = -0.848$
$R_b = 1.013$
$\delta = 21$ Aralık $= -23.45$
$n = 355$
$G_{sc} = 1367 \frac{W}{m^2}$
$\phi = 37^o$

When we entered this values in equation 10. Our result is

$$I_0 = 1.522 \times 10^7 \frac{J}{m^2}$$

This value gives the solar energy falling on the horizontal surface throughout the day. When we multiply this by R_b, we get the solar energy falling on the panel standing at that Beta angle.

$$I_{est} = I_0 \times R_b = 4.155 \times 10^7 \times 1.013 = 1.541 \times 10^7 \frac{J}{m^2}$$

And finally we multiply this result with panel efficiency and total area of panel for that beta angle. Then we reach our acquired energy for this certain beta angle.

We already know we have 106 panel for a line.

1 panel area=$0.0028\ m^2$

$total\ panel\ area$ =1 panel area× 106=$0.2968\ m^2$

η_{cell}=Panel efficiency =%29.5

$Acquired\ energy = I_{est} \times total\ panel\ area \times \eta_{cell} = 1.349 \times 10^6$ J

When I repeat this process for all beta angles and add up the energies obtained is

$$E_{total} = 1.791 \times 10^7\ J = 17.9\ MJ$$

It has been calculated that the energy to be produced daily throughout the year will vary between 17.9 and 52 MJ. In order to ensure the accuracy of our calculations, studies on the monthly average solar radiation were carried out. As can be seen in the figure below, there is a difference of more than 2.5 times between the months with the least sunshine and the months with the most sunshine. [24]

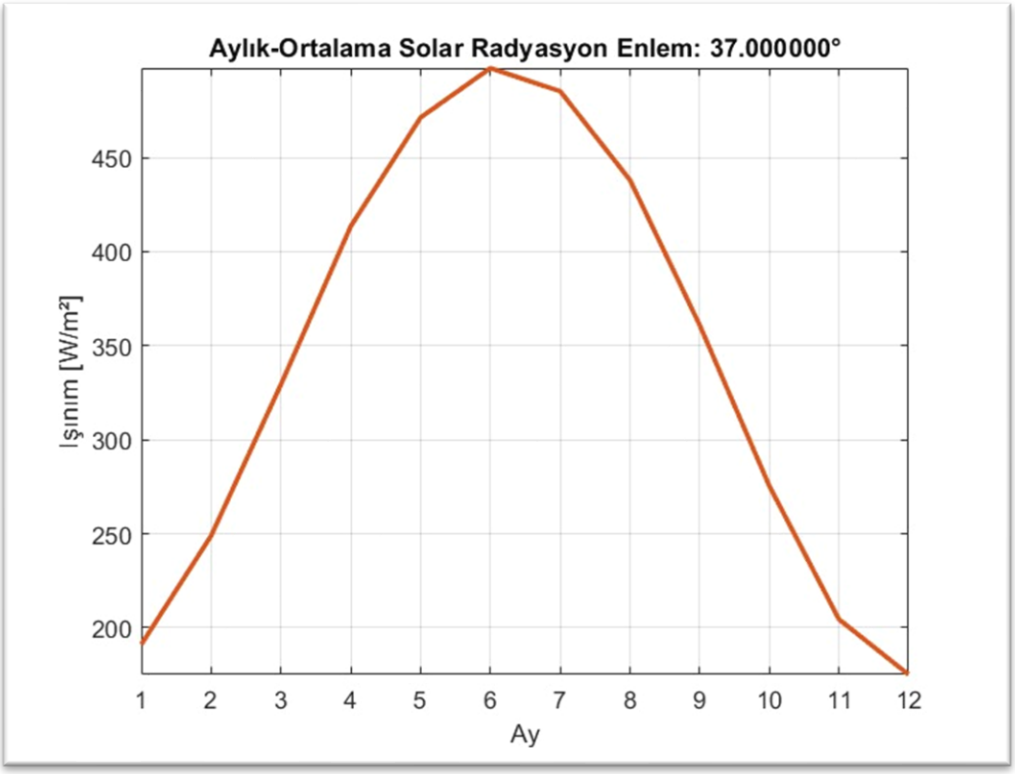

Figure 3.6 Monthly-Average Solar Radiation

The power requirement was determined to be 825 watts. Assuming an overall efficiency of the entire power generation and transmission lines as $\eta_{overall}$ =0.60, an approximate power requirement of 1375 watts is calculated.

This is equivalent to 1375 joules/s (P_{req}=1375 J/s). The energy required for approximately 10 hours of flight is:

$$E_{10h\ flight} = 10\ hours \times 60\ minutes/hour \times 60\ seconds/minute \times 1375\ joules/second$$

$$E_{10h\ flight} = 4.95 \times 107\ J$$

$$E_{10h\ flight} < E_{total}$$

Thus, it is demonstrated that the design can support uninterrupted flight for 10 hours. It should be noted that certain deviations can be expected when considering the weight of the UAV and real environmental conditions in the calculations.

4 RESULT

In this study, the main objective was to design a solar-powered UAV (Unmanned Aerial Vehicle) and develop a system that can meet its energy requirements. The focus was primarily on the wing structure and the optimal placement of solar panels on the wing.

The first step involved selecting a wing design that would not only maximize the wing surface area but also maintain the aerodynamic integrity of the UAV. The chosen wing geometry needed to strike a balance between maximizing solar panel coverage and minimizing any negative impact on the UAV's flight performance.

The calculation mentioned above section was based on the duration of a solar day, and the energy requirement was estimated for a 10-hour flight. However, for longer duration flights, additional power supplementation is needed. By incorporating a Li-Ion battery pack, the UAV can achieve a flight time of 24 hours. It is important to consider that this extended flight time will come with additional requirements, such as increased weight and other factors that need to be addressed in the design. These considerations ensure that the UAV is equipped to handle the specific demands of longer flights, allowing for extended operational capabilities.

Once the wing structure was determined, the next phase involved carefully arranging the solar panels on the wing. The goal was to achieve an efficient layout that maximized the solar energy harvesting capabilities while considering the aerodynamic aspects. Special attention was given to avoiding areas such as the leading edge and trailing edge of the wing, which could disrupt airflow and compromise the UAV's aerodynamic performance. Through detailed calculations and analysis, it was established that during a 10-hour UAV flight, the solar panels placed on the wing would generate more energy than the UAV would consume. This meant that the excess energy could be stored or used to power additional onboard systems, allowing the UAV to operate for extended periods without the need for recharging or refueling. By successfully harnessing solar energy and integrating it into the UAV's power system, the designed aircraft demonstrated the capability to perform long-duration flights without the requirement for frequent landings. This capability opens possibilities for extended surveillance, observation, and exploration missions over larger areas, reducing the need for multiple UAVs and enhancing overall operational efficiency.

5 DISCUSSON

It is important to note that the efficiency of technology and solar cells is continuously evolving. As advancements are made in the field of renewable energy, including solar power, it is expected that there will be further improvements in the efficiency of solar panels and related components. These advancements can lead to increased power generation and better energy utilization in solar-powered UAV designs.

As technology progresses, new innovations and inventions may emerge, offering even more efficient and lightweight solar cell designs. Research and development efforts in this field are likely to focus on improving solar cell efficiency, reducing weight and size, and enhancing overall system performance.

Therefore, it is crucial for future studies and designs to consider the potential advancements in technology and the evolving efficiency of solar cells. This allows for the integration of the latest developments into the UAV design, enabling longer and more efficient flights. By staying abreast of the latest advancements, researchers and engineers can continue to push the boundaries of solar-powered UAV capabilities and unlock new possibilities in the field of aerial exploration, observation, and surveillance.

6 CONCLUSION

In conclusion, the study conducted on the design and integration of solar energy in UAVs provides valuable insights and recommendations for the advancement of solar-powered UAV designs. The following key points summarize the findings and propose future directions for further improvements:

- Enhancing Solar Cell Efficiency: One of the primary goals in solar energy integration is to improve the efficiency of solar cells. This can be achieved through research and development focused on high-efficiency solar cell technologies. The integration of these advanced solar cells into UAV designs should be investigated to maximize energy conversion and optimize power generation.

- Airflow Simulations: The placement of solar cells on UAV wings can impact the airflow and aerodynamic performance. Detailed airflow simulations and analyses are crucial for assessing the effects of solar cell placement on wing aerodynamics. By considering aerodynamic considerations during solar cell integration, the UAV's overall performance and stability can be maintained or improved.

- Material Optimization: The selection of lightweight and durable materials for solar cells and wing structures is vital for achieving optimal weight reduction without compromising structural integrity. Ongoing research should focus on exploring advanced materials and composites that offer a balance between weight reduction and strength, ultimately enhancing the UAV's flight efficiency and endurance.

- Utilization for Different Applications: The designed UAV, with its low payload capacity, is well-suited for various observation and marking purposes. A significant application highlighted is the detection and timely response to wildfires, which can help mitigate forest loss by enabling prompt intervention. Further exploration of other potential applications, such as environmental monitoring or aerial surveys, should be considered to leverage the capabilities of solar-powered UAVs effectively.

In conclusion, the study underscores the importance of continuous research and development efforts in improving solar cell efficiency, conducting airflow simulations, optimizing materials, and exploring diverse applications. By addressing these aspects, solar-powered UAVs can be further optimized, leading to enhanced energy utilization, improved flight performance, and expanded operational capabilities for a wide range of beneficial applications.

Furthermore, the economic advantages of solar-powered UAVs should not be overlooked. The utilization of solar energy can significantly reduce operational costs in the long run, as sunlight is a free and abundant resource. By relying on solar power, UAVs can extend their flight durations, cover larger areas, and perform prolonged surveillance or monitoring tasks without the need for frequent refueling or battery replacement.

To fully capitalize on the potential of solar-powered UAVs, continuous collaboration between researchers, engineers, and industry experts is essential. This interdisciplinary approach will foster technological advancements, facilitate knowledge sharing, and drive innovation in solar energy integration for UAVs.

7 REFERENCES

[1] Noth, A., *Design of Solar Powered Airplanes for Continuous Flight*, Ph. D. Dissertation, Autonomous Systems Lab, ETH Zürich, Switzerland, 2008.

[2] Boucher, R. J., "Sunrise the World's First Solar-Powered Airplane." *Journal of Aircraft* Vol 22, No 10, 1985.

[3] https://i.ytimg.com/vi/LDZRVlLH6QI/maxresdefault.jpg

[4] H. Bruss, Solar Modellflug Grundlagen, Enwicklung, Praxis, Verlag für Technik und handwerk, Baden-Baden,1991

[5] Noth, A. ,(July 2008), History of Solar Flight, Autonomous Systems Lab, Swiss Federal Institute of Technology Zürich

[6] https://www.wikiwand.com/de/Icar%C3%A9_II

[7] Mermer,E., (March 2016), Conceptual Design of a Hybrid (Turbofan/Solar) powered hale UAV, Degree of Master of science Thesis, Middle East Technical University, The graduate School of Naturel and Applied Sciences, Ankara, Türkiye, 7-13

[8] "Solar HALE Drones Turn into Atmospheric Satellites", [Online]. Available: http://defense-update.com/20130813_solar_hale_atmospheric_satellites.html, last visited on March 2016.

[9] https://www.emsd.gov.hk/energyland/en/energy/renewable/solar_photovoltaic.html

[10] ZEYNEP DENİZ EZGİ, PRODUCTION OF AMORPHOUS SILICON/ P-TYPE CRYSTALLINE SILICON HETEROJUNCTION SOLAR CELLS BY SPUTTERING AND PECVD METHODS, MIDDLE EAST TECHNICAL UNIVERSITY, 2011.

[11] https://www.pv-magazine.com/2018/07/03/alta-devices-sets-28-9-efficiency-record-for-single-junction-gaas-cell/

[12] Green, M. A., Emery, K., Hishikawa, Y., Warta, W., & Dunlop, E. D. (2019). Solar cell efficiency tables (version 54). Progress in Photovoltaics: Research and Applications, 27(7), 565-575.

[13] Arghavani, M., & Goshayeshi, H. R. (2019). A Review on Recent Advances in Gallium Arsenide Solar Cells. In Nanoscale Solar Cells (pp. 105-130). Springer.

[14]Emre Yılmaz, DEVELOPMENT AND CHARACTERIZATION OF TIN BASED ANODE
MATERIALS FOR LI-ION BATTERIES, MIDDLE EAST TECHNICAL UNIVERSITY,2017.

[15] Jun Song Chen, Lynden A. Archer, and Xiong Wen (David) Lou. Sno2 hollow structures and tio2 nanosheets for lithium-ion batteries. J. Mater. Chem., 21:9912–9924, 2011

[16] Hartney,C.J., Design of a Small Solar-Powered Unmanned Aerial Vehicle, San Jose State University, August 2011,

[17] https://aerotoolbox.com/intro-wing-design/

[18] Azur Space, 32% Quadruple Junction GaAs Solar Cell Type: QJ Solar Cell 4G32C Advanced, Data Sheet, Commercial Product

[19] CESI S.p.A.— Via Rubattino, 54 I-20134 Milan, Italy, Triple-Junction Solar Cell for Space Applications (CTJ30), Data Sheet, Commercial Product-2

[20] https://gml.noaa.gov/grad/solcalc/ (Earth System Research Laboratories)

[21] Duffie, J.A., Beckman W.A., Solar Engineering of Thermal Processes Third Edition, John Wiley and Sons, 2006.

[22] Guclu Ozcan; Nafiz Alemdaroglu. Solar irradiation estimation on a solar powered uav. International Conference on Unmanned Aircraft Systems (ICUAS), Denver, USA., 2015.

[23] Ozcan, G., "Design And ManufacturingOf A Solar Powered Unmanned Air Vehicle", M.Sc Thesis, AerospaceDepartment, Middle East Technical University, Ankara, Turkey, Sept. 2015 .

[24]Gopinathan, K. (1995). Diffuse radiation models and monthly-average, daily, diffuse data for a wide latitude range. Energy, 20(7), 657–667. doi:10.1016/0360-5442(95)00004-

8 APPANDIX

8.1 Necessary MATLAB Codes

- **SolarModel.m**

```
%%% http://www.unc.edu/courses/2007fall/geog/410/001/ - lab7
function [Monthly,Hourly]=SolarModel(Latitude, airpressure_kpa)
Latitude=37
airpressure_kpa=100
lati=Latitude;
    Month=zeros(1,12);
    p=airpressure_kpa/1000; %air presSolarsure (KPa)
    Hourly=0;

    for DayOfYear=1:365
            t=0.75; % transmittance (unitless)
            S=1367; %solar constant (w/m^2)


hours=[1,2,3,4,5,6,7,8,9,10,11,12,13,14,15,16,17,18,19,20,21,22,23,24];

            hangle=(12.0-hours)*15.0*pi/180.0; % Note pi/180.0 is the factor to
convert angles in degrees in radiances.

            declangle=23.45*sin(2.0*pi*(284.0+DayOfYear)/365.0)*pi/180.0; %sun
declination angle


cosz=sin(lati*pi/180.0)*sin(declangle)+cos(lati*pi/180.0)*cos(declangle)*cos(hangl
e); %solar zenith angle / coz is an array now containing the cosine
            % of solar zenith angle for each hour listed in array hours
            cosz(cosz<0)=0; %zeroes negative angles

            m=p./(101.3*cosz); %optical airmass

            Sb=cosz*S.*(t.^m); % Sb is the beam radiation on a horizontal surface
            Sd=0.3*(1.0-t.^m)*S.*cosz; % Sd is the diffuse radiation on a
horizontal surface
            St=Sb+Sd; % St is the total radiation;
            Hourly=(Hourly+St);
            Irradiance_Wm2 = mean(St);

        %Jan = 1 - 31 (31)
        %Feb = 32 - 59 (28)
        %Mar = 60 - 90 (31)
        %Abr = 91 - 120 (30)
        %May = 121 - 151 (31)
        %Jun = 152 - 181 (30)
        %Jul = 182 - 212 (31)
        %Aug = 213 - 243 (31)
        %Sep = 244 - 273 (30)
        %Oct = 274 - 304 (31)
        %Nov = 305 - 334 (30)
        %Dec = 335 - 365 (31)

        if DayOfYear <= 31
            Month(1,1) = Month(1,1)+Irradiance_Wm2;
        elseif DayOfYear >=32 && DayOfYear <=59
```

```
            Month(1,2) = Month(1,2)+Irradiance_Wm2;
        elseif DayOfYear >=60 && DayOfYear <=90
            Month(1,3) = Month(1,3)+Irradiance_Wm2;
        elseif DayOfYear >=91 && DayOfYear <=120
            Month(1,4) = Month(1,4)+Irradiance_Wm2;
        elseif DayOfYear >=121 && DayOfYear <=151
            Month(1,5) = Month(1,5)+Irradiance_Wm2;
        elseif DayOfYear >=152 && DayOfYear <=181
            Month(1,6) = Month(1,6)+Irradiance_Wm2;
        elseif DayOfYear >=182 && DayOfYear <=212
            Month(1,7) = Month(1,7)+Irradiance_Wm2;
        elseif DayOfYear >=213 && DayOfYear <=243
            Month(1,8) = Month(1,8)+Irradiance_Wm2;
        elseif DayOfYear >=244 && DayOfYear <=273
            Month(1,9) = Month(1,9)+Irradiance_Wm2;
        elseif DayOfYear >=274 && DayOfYear <=304
            Month(1,10) = Month(1,10)+Irradiance_Wm2;
        elseif DayOfYear >=305 && DayOfYear <=334
            Month(1,11) = Month(1,11)+Irradiance_Wm2;
        elseif DayOfYear >=335 && DayOfYear <=365
            Month(1,12) = Month(1,12)+Irradiance_Wm2;
        end
    end
    Month(1,1)=Month(1,1)/31;
    Month(1,2)=Month(1,2)/28;
    Month(1,3)=Month(1,3)/31;
    Month(1,4)=Month(1,4)/30;
    Month(1,5)=Month(1,5)/31;
    Month(1,6)=Month(1,6)/30;
    Month(1,7)=Month(1,7)/31;
    Month(1,8)=Month(1,8)/31;
    Month(1,9)=Month(1,9)/30;
    Month(1,10)=Month(1,10)/31;
    Month(1,11)=Month(1,11)/30;
    Month(1,12)=Month(1,12)/31;
    Monthly=Month;
    Hourly=Hourly/365;
    plot(Monthly,'LineWidth',2);
    monthlyTitle=sprintf('Aylık-Ortalama Solar Radyasyon Enlem: %f°',Latitude);
    title(monthlyTitle,'FontWeight','Bold')
    xlabel('Ay')
    ylabel('Işınım [W/m²]')
    imin = min(Monthly);
    imax = max(Monthly);
    xlim([1 12])
    ylim([imin imax])
    grid on
    hold on

end
```

- **Daylength.m**

```
function [mind,maxd]=daylength(L)

for J=1:365
    %CBM Model
    theta=0.2163108+2*atan(0.9671396*tan(0.00860*(J-186))); %revolution angle from
day of the year
    P = asin(0.39795*cos(theta)); %sun declination angle
    %daylength (plus twilight)-
    L=40;
    p=0.8333; %sunrise/sunset is when the top of the sun is apparently even with
horizon
    D(J) = 24 - (24/pi) *
acos((sin(p*pi/180)+sin(L*pi/180)*sin(P))/(cos(L*pi/180)*cos(P)));
end
    avg=mean(D);
    mind=min(D)
    meand=mean(D);
    maxd=max(D)
    plot(D,'LineWidth',2)
    hold on
    %hline=refline([0 avg]);
    imin = min(D);
    imax = max(D);
    xlim([1 365])
    ylim([imin imax])
    xlabel('Day of Year')
    ylabel('Hours')
    grid on
    title('Day Length','FontWeight','Bold')
    %text(120,avg-0.2,strcat('   Average Day Length:     ',num2str(meand), '
h'),'FontWeight','Bold','FontSize',8)

end
```

- **SolarHESAP_1.m**

```
clc
clear all

w=0.07; %width of solar cell
l=0.04; %length of solar cell
area=w*l; %solar cell area
solarcellefficiency=0.295;
horizontalcellno=106;
B1=18.5;  %beta angles of example
B2=0;     %beta angles of example
B3=15;    %beta angles of example

B1=31;
B2=18.5;
B3=12;
B4=6.5;
B5=3;
B6=-2;
B7=-5.3;
B8=-7.2;
B9=-9;
B10=-10.8;
B11=-12.5;
B12=-14;
B13=-15.5;
B14=16;


% Our Bheta Angles 28.2 15.2 8.2 2.2 3.3 5.8 8.4 10.8 12.3 14.8 16.8 18.8
G=1367; % Solar Constant W/m^2
n=355; % June 11th day number
dec=23.1; %declination angle from table
    % declination angle formula
dec=23.45*sind(360*(284+n)/365);
dec=round(dec,3);
lat=37; % latitude
ws=7.50 ;          % time of the day converted to degrees 12:00 is 0 each hour
15degree
w1=15*(ws-12);
wf=17.25;
w2=15*(wf-12);
costhe1= sind(dec)*sind(lat-B1)+cosd(dec)*cosd(lat-B1)*cosd(w2-w1);
costhez1=sind(dec)*sind(lat)+cosd(dec)*cosd(lat)*cosd(w2-w1);
Rb1=costhe1/costhez1;
Rb1=round(Rb1,3);
% Hourly integrated Solar İrradiation
I0=(12*3600/pi)*G*(1+0.033*cosd((360*n/365)))*(cosd(lat)*cosd(dec)*(sind(w2)-
sind(w1))+((pi*(w2-w1)/180*sind(dec))*sind(lat)));
Iest1=I0*area*Rb1*horizontalcellno*solarcellefficiency;

%Second Beta Angle

costhe2= sind(dec)*sind(lat-B2)+cosd(dec)*cosd(lat-B2)*cosd(w2-w1);
costhez2=sind(dec)*sind(lat)+cosd(dec)*cosd(lat)*cosd(w2-w1);
Rb2=costhe2/costhez2;
Rb2=round(Rb2,3);
% Hourly integrated Solar İrradiation
```

```
I02=(12*3600/pi)*G*(1+0.033*cosd((360*n/365)))*(cosd(lat)*cosd(dec)*(sind(w2)-
sind(w1))+((pi*(w2-w1)/180*sind(dec))*sind(lat)));
Iest2=I02*area*Rb2*horizontalcellno*solarcellefficiency;

% Third Beta Angle

costhe3= sind(dec)*sind(lat-B3)+cosd(dec)*cosd(lat-B3)*cosd(w2-w1);
costhez3=sind(dec)*sind(lat)+cosd(dec)*cosd(lat)*cosd(w2-w1);
Rb3=costhe3/costhez3;
Rb3=round(Rb3,3);
% Hourly integrated Solar İrradiation
I03=(12*3600/pi)*G*(1+0.033*cosd((360*n/365)))*(cosd(lat)*cosd(dec)*(sind(w2)-
sind(w1))+((pi*(w2-w1)/180*sind(dec))*sind(lat)));
Iest3=I03*Rb3;
Iest3=I03*Rb3*area*horizontalcellno*solarcellefficiency;
%fourth

costhe4= sind(dec)*sind(lat-B1)+cosd(dec)*cosd(lat-B4)*cosd(w2-w1);
costhez4=sind(dec)*sind(lat)+cosd(dec)*cosd(lat)*cosd(w2-w1);
Rb4=costhe4/costhez4;
Rb4=round(Rb4,3);
% Hourly integrated Solar İrradiation
I04=(12*3600/pi)*G*(1+0.033*cosd((360*n/365)))*(cosd(lat)*cosd(dec)*(sind(w2)-
sind(w1))+((pi*(w2-w1)/180*sind(dec))*sind(lat)));
Iest4=I04*area*Rb4*horizontalcellno*solarcellefficiency;

%fifth

costhe5= sind(dec)*sind(lat-B5)+cosd(dec)*cosd(lat-B5)*cosd(w2-w1);
costhez5=sind(dec)*sind(lat)+cosd(dec)*cosd(lat)*cosd(w2-w1);
Rb5=costhe5/costhez5;
Rb5=round(Rb5,3);
% Hourly integrated Solar İrradiation
I05=(12*3600/pi)*G*(1+0.033*cosd((360*n/365)))*(cosd(lat)*cosd(dec)*(sind(w2)-
sind(w1))+((pi*(w2-w1)/180*sind(dec))*sind(lat)));
Iest5=I05*area*Rb5*horizontalcellno*solarcellefficiency;

%sixth

costhe6= sind(dec)*sind(lat-B6)+cosd(dec)*cosd(lat-B6)*cosd(w2-w1);
costhez6=sind(dec)*sind(lat)+cosd(dec)*cosd(lat)*cosd(w2-w1);
Rb6=costhe6/costhez6;
Rb6=round(Rb6,3);
% Hourly integrated Solar İrradiation
I06=(12*3600/pi)*G*(1+0.033*cosd((360*n/365)))*(cosd(lat)*cosd(dec)*(sind(w2)-
sind(w1))+((pi*(w2-w1)/180*sind(dec))*sind(lat)));
Iest6=I06*area*Rb6*horizontalcellno*solarcellefficiency;

%seventh

costhe7= sind(dec)*sind(lat-B7)+cosd(dec)*cosd(lat-B7)*cosd(w2-w1);
costhez7=sind(dec)*sind(lat)+cosd(dec)*cosd(lat)*cosd(w2-w1);
Rb7=costhe7/costhez7;
Rb7=round(Rb7,3);
% Hourly integrated Solar İrradiation
I07=(12*3600/pi)*G*(1+0.033*cosd((360*n/365)))*(cosd(lat)*cosd(dec)*(sind(w2)-
sind(w1))+((pi*(w2-w1)/180*sind(dec))*sind(lat)));
Iest7=I07*area*Rb7*horizontalcellno*solarcellefficiency;
```

```
%eigthth

costhe8= sind(dec)*sind(lat-B8)+cosd(dec)*cosd(lat-B8)*cosd(w2-w1);
costhez8=sind(dec)*sind(lat)+cosd(dec)*cosd(lat)*cosd(w2-w1);
Rb8=costhe8/costhez8;
Rb8=round(Rb8,3);
% Hourly integrated Solar İrradiation
I08=(12*3600/pi)*G*(1+0.033*cosd((360*n/365)))*(cosd(lat)*cosd(dec)*(sind(w2)-
sind(w1))+((pi*(w2-w1)/180*sind(dec))*sind(lat)));
Iest8=I08*area*Rb8*horizontalcellno*solarcellefficiency;

%ninth

costhe9= sind(dec)*sind(lat-B9)+cosd(dec)*cosd(lat-B9)*cosd(w2-w1);
costhez9=sind(dec)*sind(lat)+cosd(dec)*cosd(lat)*cosd(w2-w1);
Rb9=costhe9/costhez9;
Rb9=round(Rb9,3);
% Hourly integrated Solar İrradiation
I09=(12*3600/pi)*G*(1+0.033*cosd((360*n/365)))*(cosd(lat)*cosd(dec)*(sind(w2)-
sind(w1))+((pi*(w2-w1)/180*sind(dec))*sind(lat)));
Iest9=I09*area*Rb9*horizontalcellno*solarcellefficiency;

%tenth

costhe10= sind(dec)*sind(lat-B10)+cosd(dec)*cosd(lat-B10)*cosd(w2-w1)
costhez10=sind(dec)*sind(lat)+cosd(dec)*cosd(lat)*cosd(w2-w1)
Rb10=costhe10/costhez10;
Rb10=round(Rb10,3)
% Hourly integrated Solar İrradiation
I010=(12*3600/pi)*G*(1+0.033*cosd((360*n/365)))*(cosd(lat)*cosd(dec)*(sind(w2)-
sind(w1))+((pi*(w2-w1)/180*sind(dec))*sind(lat)));
Iest10=I010*area*Rb10*horizontalcellno*solarcellefficiency;

%eleventh

costhe11= sind(dec)*sind(lat-B11)+cosd(dec)*cosd(lat-B11)*cosd(w2-w1);
costhez11=sind(dec)*sind(lat)+cosd(dec)*cosd(lat)*cosd(w2-w1);
Rb11=costhe11/costhez11;
Rb11=round(Rb11,3);
% Hourly integrated Solar İrradiation
I011=(12*3600/pi)*G*(1+0.033*cosd((360*n/365)))*(cosd(lat)*cosd(dec)*(sind(w2)-
sind(w1))+((pi*(w2-w1)/180*sind(dec))*sind(lat)));
Iest11=I011*area*Rb11*horizontalcellno*solarcellefficiency;

%twelveth

costhe12= sind(dec)*sind(lat-B12)+cosd(dec)*cosd(lat-B12)*cosd(w2-w1);
costhez12=sind(dec)*sind(lat)+cosd(dec)*cosd(lat)*cosd(w2-w1);
Rb12=costhe12/costhez12;
Rb12=round(Rb12,3);
% Hourly integrated Solar İrradiation
I012=(12*3600/pi)*G*(1+0.033*cosd((360*n/365)))*(cosd(lat)*cosd(dec)*(sind(w2)-
sind(w1))+((pi*(w2-w1)/180*sind(dec))*sind(lat)));
Iest12=I012*area*Rb12*horizontalcellno*solarcellefficiency;

%thirteenth

costhe13= sind(dec)*sind(lat-B13)+cosd(dec)*cosd(lat-B13)*cosd(w2-w1);
costhez13=sind(dec)*sind(lat)+cosd(dec)*cosd(lat)*cosd(w2-w1);
```

```
Rb13=costhe13/costhez13;
Rb13=round(Rb13,3);
% Hourly integrated Solar İrradiation
I013=(12*3600/pi)*G*(1+0.033*cosd((360*n/365)))*(cosd(lat)*cosd(dec)*(sind(w2)-
sind(w1))+((pi*(w2-w1)/180*sind(dec))*sind(lat)));
Iest13=I013*area*Rb13*horizontalcellno*solarcellefficiency;

%fourteenth

costhe14= sind(dec)*sind(lat-B14)+cosd(dec)*cosd(lat-B14)*cosd(w2-w1);
costhez14=sind(dec)*sind(lat)+cosd(dec)*cosd(lat)*cosd(w2-w1);
Rb14=costhe14/costhez14;
Rb14=round(Rb14,3);
% Hourly integrated Solar İrradiation
I014=(12*3600/pi)*G*(1+0.033*cosd((360*n/365)))*(cosd(lat)*cosd(dec)*(sind(w2)-
sind(w1))+((pi*(w2-w1)/180*sind(dec))*sind(lat)));
Iest14=I014*area*Rb14*horizontalcellno*solarcellefficiency;


Totalenergy=Iest1+Iest2+Iest3+Iest4+Iest5+Iest6+Iest7+Iest8+Iest9+Iest10+Iest11+Ie
st12+Iest13+Iest14
```